Molecular dynamics simulations of ionscattering on a supported rhodium cluster

den Otter, W.K.

Award date:
1993

Molecular dynamics simulations of ionscattering on a supported rhodium cluster

W.K. den Otter

March 1993.

This work was done at the Philips Research Laboratories, under the supervision of Prof.dr. H.H. Brongersma[1] and Dr. H. Feil[2].

[1]Department of Physics
Eindhoven University of Technology
P.O. Box 513
5600 MB Eindhoven.

[2]Theoretical Physics Department
Philips Research Laboratories
P.O. Box 80.000
5600 JA Eindhoven

Summary

A highly active rhodium catalyst can be made by depositing a small amount of rhodium on a sponge like carrier, for instance SiO_2 or Al_2O_3. Due to the strong cohesive forces compared to the adhesive forces, the rhodium will grow into clusters. In this study we focus on clusters of about 15 Å in diameter. Several surface sensitive techniques are being applied to study these surfaces, two of which are discussed in detail. In both these methods low energy ions (0.1 - 10 keV) are directed towards the sample. One either detects the back-scattered ions (Low Energy Ion Scattering (LEIS)) or the sputtered atoms (Secondary Ion Mass Spectrometry (SIMS)). From these measurements the qualitative surface composition of the sample is determined. The problem lies at the quantification of the experimental results. Part of the problem is of mechanical nature: what will be the influence of the impinging ion on the cluster? The existing sputter theories for bulk samples are in reasonable agreement with experiment, but their correctness for sputtering from a small cluster is questionable.

In this study the scattering of ions on rhodium clusters is numerically simulated using Molecular Dynamics (MD). In MD the positions (and velocities) of all involved atoms at time t_0 are used to calculate their mutual interactions. Integrating these forces over a timestep Δt gives the positions and velocities at time $t_0 + \Delta t$. This iterative process is repeated 2500 times, to cover a timespan of a couple of picoseconds. MD simulations are based on pure classical mechanics, the quantum mechanical aspect of the scattering process are incorporated in the interaction potential. For the rhodium-rhodium interaction the Embedded Atom Method (EAM) was used. This many-body potential was originally designed for application on lattice-like situations, so two-body potentials have been added for a correct description of the hard collisions and the sputtered dimers.

The shape of the rhodium clusters is still a subject of discussion. We chose a cluster with an icosahedral shape, containing 147 atoms. The cluster was placed on the (111) surface of a three layer thick rhodium support. This cluster-support combination is fairly stable with the EAM potential.

The cluster and support were bombarded with helium, neon and argon with kinetic energies of 0.5, 2.0 and 5.0 keV. The clusters are indeed fragile, nearly each cluster that is being hit loses one or more atoms. The obtained sputter yields for ions impinging in (or within interaction reach of) the cluster are considerably higher than those for bulk rhodium. Other striking differences are the higher average kinetic energies of the sputtered atoms and their angular distribution. Just like for bulk, the majority of the sputtered atoms originates from the surface layer.

Table of contents

1 Introduction

1.1 Surface science

Surface science has developed enormously in the last two decades. It has proven to give unique and valuable information on the behaviour of solids at their surfaces. This knowledge is applied in various fields of industrial and academic interest, such as micro electronics and heterogeneous catalysis.

During this period a whole range of surface analysis techniques has been developed. In this study two techniques are discussed, Low Energy Ion Scattering (LEIS) and Secondary Ion Mass Spectrometry (SIMS). The principles of these techniques are discussed in paragraph 1.3. The problem addressed here is the quantification of the measured data. For single crystals this problem is quite well understood, but for more complicated surfaces not much is known. In the following paragraph the surface of interest is introduced.

1.2 Catalysis

A catalyst can be described as a substance which increases the rate of a chemical reaction, without being consumed. They are used to increase the production rate and/or soften the conditions at which a reaction takes place. Another advantage is the selective enhancement of a desired reaction, reducing the amount of unwanted by-products.

Often the catalyst is a solid, while the reactants are gaseous or liquid. This is called heterogeneous catalysis. Since most of the reactant atoms will not penetrate into a solid only the surface layer will catalyse the reaction. A higher activity can thus be obtained by increasing the surface area. A common method is to deposit a thin active layer on top of a support with a high specific surface area. Frequently used supports are grains of the porous alumina (Al_2O_3) and silica (SiO_2), with specific surface areas of the order of several hundreds of square meters per gram. Their small pores (about 5 Å diameter, depending on the structure) can suppress unwanted side reactions that produce too large molecules. They are also usable as molecular sieves. A problem is how to deposit the active layer over the entire inner surface of the support and not merely over the outermost region. Several methods have been proposed and are being used to solve this problem[1].

An industrial method for the deposition of rhodium on a support is wetting the support with an aqueous solution of $RhCl_3.xH_2O$. After adsorption on the support and drying, the bound rhodium chloride is transformed into metallic rhodium by reduction in hydrogen at 300°C. The various stages of this process have been studied by Van den Oetelaar[2], using X-ray Photoemission Spectroscopy (XPS), Rutherford Backscattering Spectrometry (RBS) and Secondary Ion Mass Spectrometry (SIMS). The rhodium-rhodium bond is stronger than the rhodium-support bond, so the deposited rhodium tends to sinter into clusters during annealing. The sizes of the clusters vary from a couple of atoms up to several thousands (10 nm diameter and bigger), depending on the preparation method. These clusters are

clearly distinguishable in Transmission Electron Microscopy[3] (TEM). They still show catalytic behaviour, with activities depending on their size and the support[4].

1.3 Surface analysis techniques

1.3.1 Introduction

Many techniques are being used to analyse surfaces[5]. We focus on two techniques that are being used at the Eindhoven University of Technology. In both methods ions are accelerated to a kinetic energy of the order of a keV and directed towards the sample. A small fraction of the incoming ions is backscattered by the surface atoms. From their energy and angle distribution the surface composition is determined. This technique is known as Low Energy Ion Scattering (LEIS). In the scattering process the ion transfers its energy to the sample, this energy then spreads out. Some atoms may gain enough energy to escape from the bulk. In Secondary Ion Mass Spectrometry (SIMS) these sputtered atoms are detected to determine the atomic composition of the surface layers. These experiments are performed in ultra high vacuum ($< 10^{-9}$mbar), to keep the surface clean and to avoid deflection and neutralization of the ions.

1.3.2 LEIS

In Low Energy Ion Scattering (LEIS) or Ion Scattering Spectroscopy (ISS) the energy and angle distribution of the backscattered ions are measured. Imagine an ion of initial energy E_i moving towards a motionless target atom, as in figure 1.1. If the collision process is elastic, conservation of energy and momentum may be used to derive the final energy of

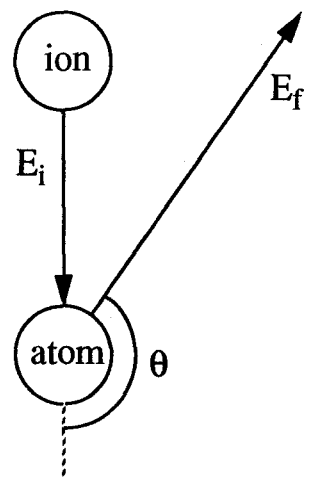

Fig. 1.1 An ion is scattered from a target atom over an angle θ. In this process the energy of the ion reduces from E_i down to E_f.

the ion,

$$E_f = E_i\left(\frac{\cos\theta \pm \sqrt{q^2 - \sin^2\theta}}{1+q}\right)^2, \qquad (1.1)$$

where $q = m_{atom}/m_{ion}$ and θ is the scattering angle. For scattering angles over 90° only the plus sign gives a physical solution. By measuring the kinematic factor E_f/E_i and θ of a scattered ion the mass of the scattering target atom can be determined. Although not entirely correct, ions scattered from the surface atoms of a solid show a very similar angle versus energy relation. If this equation is applied on ions scattered from a sample the possibility of detecting ions that were scattered by more than one atom must be ruled out. This is achieved by using noble gas ions. Because of their high electron negativity they have a high neutralization probability: in a binary collision about 99.9% neutralizes. If an ion reaches the detector it has very likely been scattered only once. This makes LEIS a surface sensitive technique: ions that have been scattered from atoms below the surface have been in the electron gas of the bulk considerably longer than ions scattered from the surface and are therefore more likely to be neutralized. LEIS has been applied on a carried rhodium catalyst[6]. Figure 1.2 shows measurements on carried platina-palladium (ratio 4:1) clusters[7].

At the physics department of the TUE a new apparatus has been designed and built,

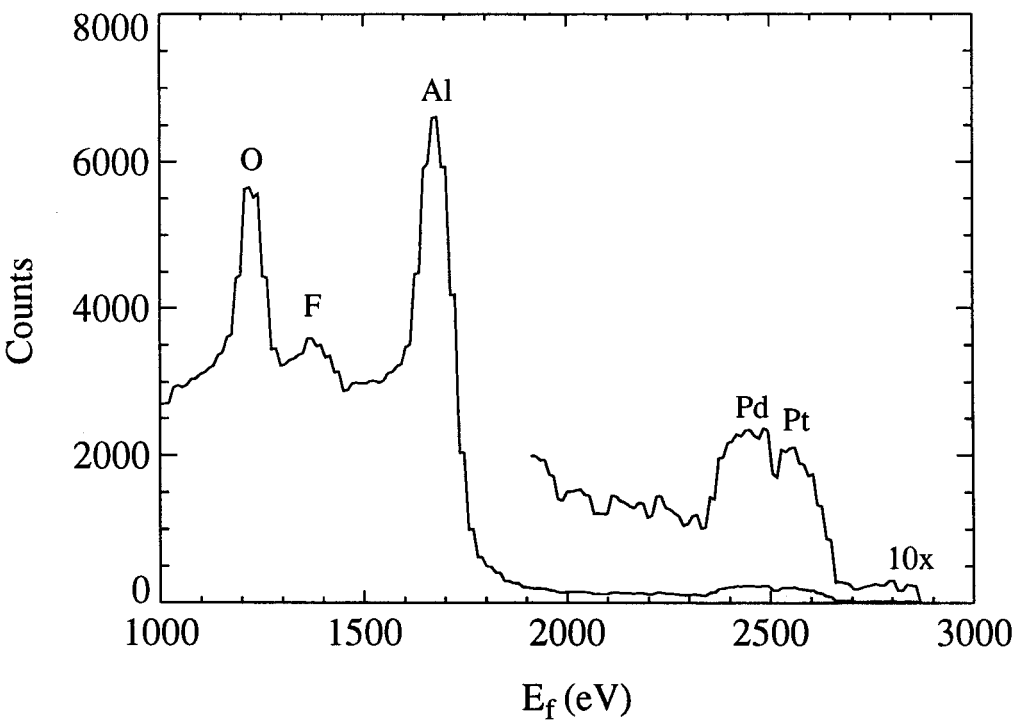

Fig. 1.2 LEIS spectrum of Pt-Pd clusters on Al_2O_3. Incident $^4He^+$ with an energy of 3.0 keV at a current of 240 nA.

the Energy and Angular Resolved Ion Scattering Spectrometer (EARISS)[8]. It detects simultaneously the energy and the azimuth angle of ions scattered over 145°. The system is much more sensitive than the previously used systems. The main advantage is that much lower ion-doses are required to get a sufficient signal to noise ratio.

1.3.3 SIMS

Once an ion reaches the sample it can be scattered on the bulk atoms. In a series of hard and soft collisions the ion loses (part of) its kinetic energy. This series may start at or near the surface, but it could also start deep inside the bulk. The later is more likely for high energetic ions (MeV) as used in Rutherford Backscattering Spectrometry (RBS), since the scattering cross section decreases with increasing kinetic energy. The atom(s) from which the ion is scattered gain an excess energy and start moving around, initiating a cascade of moving atoms. Some 250 femtosecond after the primary recoil the recoil energy has spread out over 100 atoms, the sample has locally melted.

If the cascade takes place near the surface some atoms may gain enough energy to escape from the sample into the vacuum. Most of these atoms are neutral, but some do have a positive or negative charge. If they reach the detector their mass (see figure 1.3), kinetic energy and angular distribution can be measured. Depending on the charge of the analysed

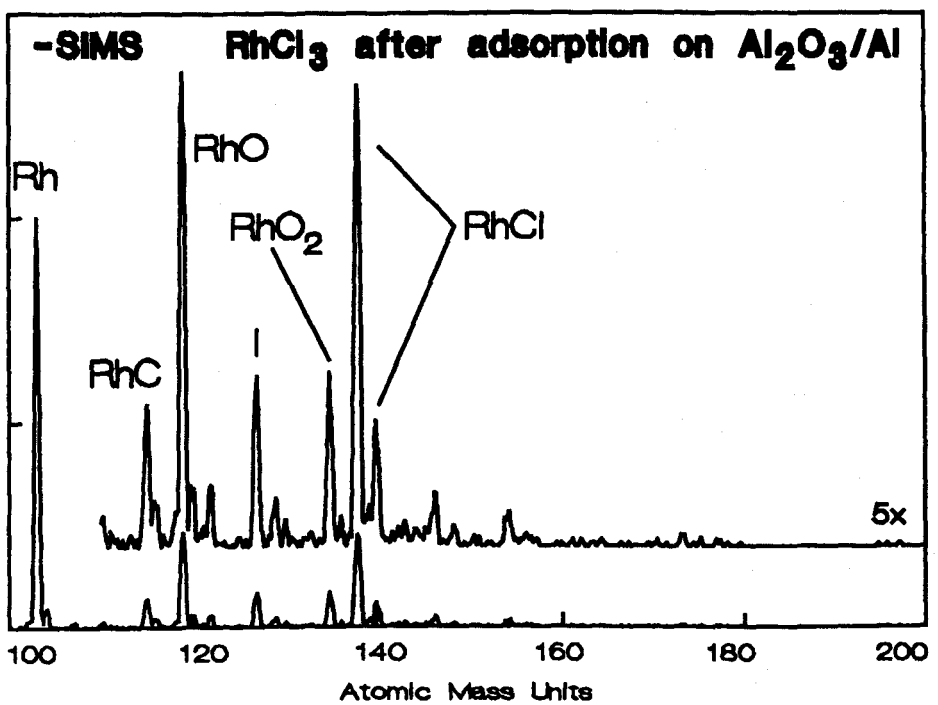

Fig. 1.3 SIMS spectrum of negative ions sputtered from rhodium chloride deposited on alumina[2]. The double RhCl peak is the result of two chlorine isotopes.

atoms this technique is called Secondary Ion Mass Spectrometry (SIMS) or Secondary Neutral Mass Spectrometry (SNMS). Sometimes entire molecules are sputtered from the sample, which gives insight in the chemical bonds present at the surface (assuming that these molecules were not formed in the vacuum). Qualitatively SIMS is a very useful technique, capable of detecting parts per million for some elements. But because of the complex nature of the collision cascade[9] it is tedious to get quantitative results.

SIMS has been extensively used and simulated for several surfaces of bulk rhodium by Garrison, Winograd and co-workers[10,11]. They calculated for 1 keV argon a yield (average number of sputtered atoms per ion) of about 2 for Rh (100) and about 3.5 for Rh (111). The angular distribution of the sputtered atoms reflects the structure of the surface. In the (100) surface some 89% of the sputtered atoms originates from the surface layer. At the chemistry department of the TUE this technique is being applied on rhodium clusters[2], for instance to study the various stages in the deposition process of the carried clusters.

1.4 Measuring the clusters

Inherent to SIMS and LEIS the bombarding ions damage a small area of the sample. If a second ion impinges in a previously hit area it will very likely experience an environment that differs from the original (undamaged) situation. In so-called static experiments this is avoided by using low ion-doses, so each ion experiences a 'fresh' area. The problem then is what doses are permitted for static conditions. Some materials - like semiconductors and polymers - are very sensitive. Others - like copper- recuperate because of the high atomic mobilities at room temperature. One may expect a rhodium cluster to be very fragile. As a rough estimation suppose that a 3 keV ion deposits all its energy in a single cluster of 150 atoms. The energy per atom then increases on the average by 20 eV (the cohesive energy for bulk rhodium is 5.75 eV) and the cluster will explode. If however the cluster manages to pass part of the energy on to the support or if some high energetic atoms are sputtered the result might be less disastrous. The goal of this study will be to determine the influence of the ion bombardment on the cluster.

Another interesting topic is how clusters that contain a mixture of atoms (e.g. platina and palladium, as in figure 1.2) will respond to an ion bombardment. Often one of the constituents dominates in the outermost layer. When sputtering from a bulk sample the surface layer is removed, but the layers underneath remain more or less intact. This is taken advantage of to measure the depth profile of a sample[12]. If clusters show the same preference to sputter surface atoms, we could 'peel' the cluster and look at its interior. The simulations might give an indication whether this is possible or not.

2 Theory and methods

2.1 Introduction

In order to obtain quantitative information on the surface composition via LEIS or SIMS we need to know some details of the collision processes that take place, like the neutralization probability and the scattering cross section. Since noble gas ions neutralize quickly we will assume in the calculations that the incident 'ion' is neutral and do not take into account the charge exchange processes. We will still use the name 'ion' though. The remaining prerequisite for quantification of the collision process is the interaction potential, as discussed in paragraph 2.5.

If the interactions between the atoms are known their trajectories can be calculated. A relatively simple method is the Binary Collision Approximation (BCA), in which the trajectory of the ion is described by a series of interactions between the ion and a single atom. In the more extended Molecular Dynamics (MD) the trajectories of all atoms are calculated and many body interactions are allowed.

2.2 The binary collision approximation

Assume that we have a convenient potential that depends only on the interatomic distances. With this potential the binary collision can be solved analytically. In the centre of mass (CM) system energy conservation gives

$$\frac{\mu}{2}(\dot{r}^2 + r^2\dot{\varphi}^2) + V(r) = E_{cm} = \frac{\mu}{2}v_d^2, \tag{2.1}$$

where $\mu = m_i m_a / (m_i + m_a)$ is the effective mass. The line connecting the ion and the atom has length r at an angle of φ with the horizon, as in figure 2.1. The velocity v_d denotes the difference between the initial velocities of the ion and the atom. If they did not interact they would pass each other at a minimum distance b, the impact parameter. Combining energy conservation with conservation of angular momentum

$$\mu r^2\dot{\varphi} = |\boldsymbol{L}_{cm}| = -\mu b v_d \tag{2.2}$$

we arrive at an expression for $\dot{r}$. Dividing eq. 2.2 by $\dot{r}$ gives $d\theta/dr$, and after integration over r an expression for the scattering angle is found,

$$\theta_{cm} = \pi - 2b\int_R^\infty [r^2 g(r)]^{-1} dr, \tag{2.3}$$

where

$$g(r) = \sqrt{1 - \frac{V(r)}{E_{cm}} - \frac{b^2}{r^2}}. \tag{2.4}$$

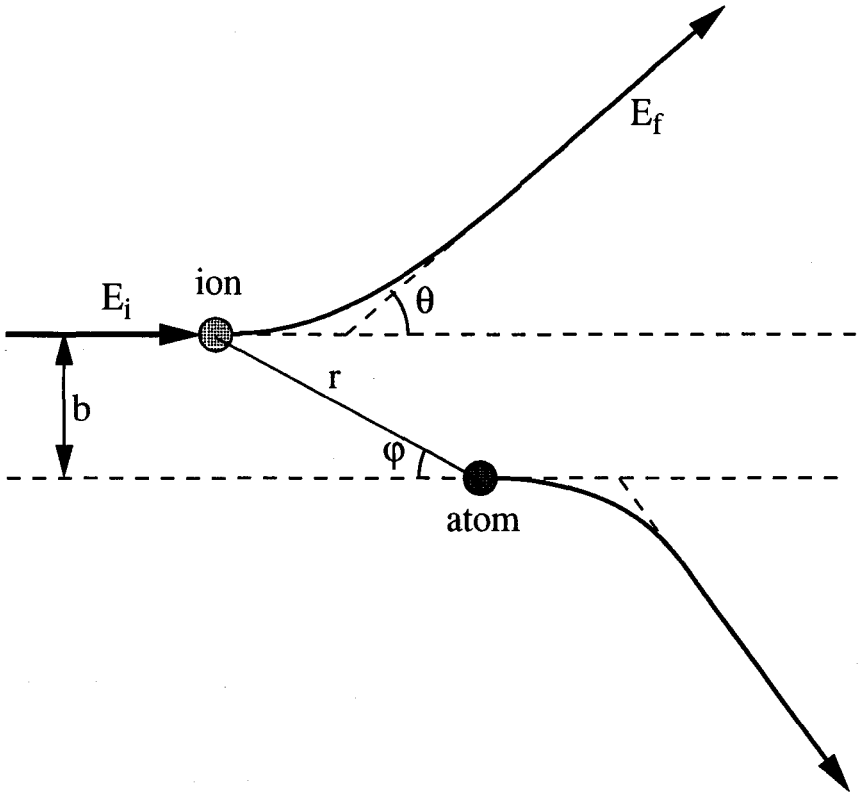

Fig. 2.1 Ion scattered from an atom. The scattering angle θ depends on the impact-parameter b.

The minimum distance R between the ion and the atom is given by $g(R) = 0$. At this point $\dot{r}$ changes its sign. Solving eq. 2.3 is tedious, but it can be done exactly for some potentials, like the Coulomb potential.

In the Binary Collision Approximation (BCA) the path of the ion (and the scattering atom as it proceeds) through the sample is regarded as a series of these binary collisions. This approximation is valid if the ion interacts with only one atom at a time and if this atom does not interact with its neighbours. That is the case if the energy of the ion is much higher than the interaction energies in the sample. Imagine an energetic ion moving around inside the sample. The ion will be scattered on each atom that comes close to its path. If the impact parameter is known the final energy and direction of the ion can be derived. We then look for the next scattering nucleus, and so on. For simulation of LEIS this works well[13]. At lower kinetic energies though, many body interactions become more and more important, breaking down the assumptions of the BCA. It is these low energy collisions that are important in the sputtering process.

2.3 Molecular dynamics

For more complicated collisions with multiple particle interactions, as needed for determining the damage of the sample, the BCA model fails. In molecular dynamics (MD) the trajectories of all atoms are calculated as a function of time, taking many body interactions into account. A good overview of its possibilities and the frequently used methods can be found in the book by Allen and Tildesley[14]. Also very useful is the overview by Eckstein[15], focusing on ion-solid simulations. We will describe the basics of the technique.

Imagine at time t_0 a set of N atoms, at positions $\bar{r}_i(t_0)$ and with velocities $\bar{v}_i(t_0)$, $1 \le i \le N$. The upperscores ($\bar{}$) indicate that these values are exact, or as accurate as possible. The positions at time $t_1 = t_0 + \Delta t$ are given by integration of the velocity over time,

$$\bar{r}_i(t_1) = \bar{r}_i(t_0) + \int_{t_0}^{t_1} \bar{v}_i(t')\,dt'. \tag{2.5}$$

The velocities are also a function of time,

$$\bar{v}_i(t') = \bar{v}_i(t_0) + \int_{t_0}^{t'} \bar{a}_i(t'')\,dt''. \tag{2.6}$$

The acceleration $\bar{a}_i(t)$ is caused by the interaction of atom i with its neighbours,

$$m_i \bar{a}_i(t) = \bar{F}_i(t) = -\nabla_{\bar{r}_i} V(\bar{r}_1(t), \bar{r}_2(t), \ldots, \bar{r}_N(t)), \tag{2.7}$$

where the derivative of the potential was taken with respect to $\bar{r}_i$. The potential may not only depend on the interatomic distances (like in eq. 2.1) but also on their relative positions. One might even add a velocity or time dependence. The problem lies in the self consistent solution of this set of equations. The only way of doing this is by numerical integration.

In molecular dynamics as well as in the binary collision approximation the classical equation of motion are used. The quantum mechanical aspects of the collision are described by the potentials, see paragraph 2.5.

2.4 The code

A numerical integration method is implemented in a fortran-77 program to be compiled and run on a SiliconGraphics R4000-50 GTX. This required a minor revision of the code used by Garrison *et al.*[10], and by Feil *et al.*[16]. The general structure of the code is given by the flowchart of figure 2.2. In the following paragraphs the various parts of the code are explained in detail.

2.4.1 The support

In a catalyst the active rhodium is deposited on a support, silica (SiO_2) or alumina (Al_2O_3), because of their high specific surface areas. There is not yet an adequate potential

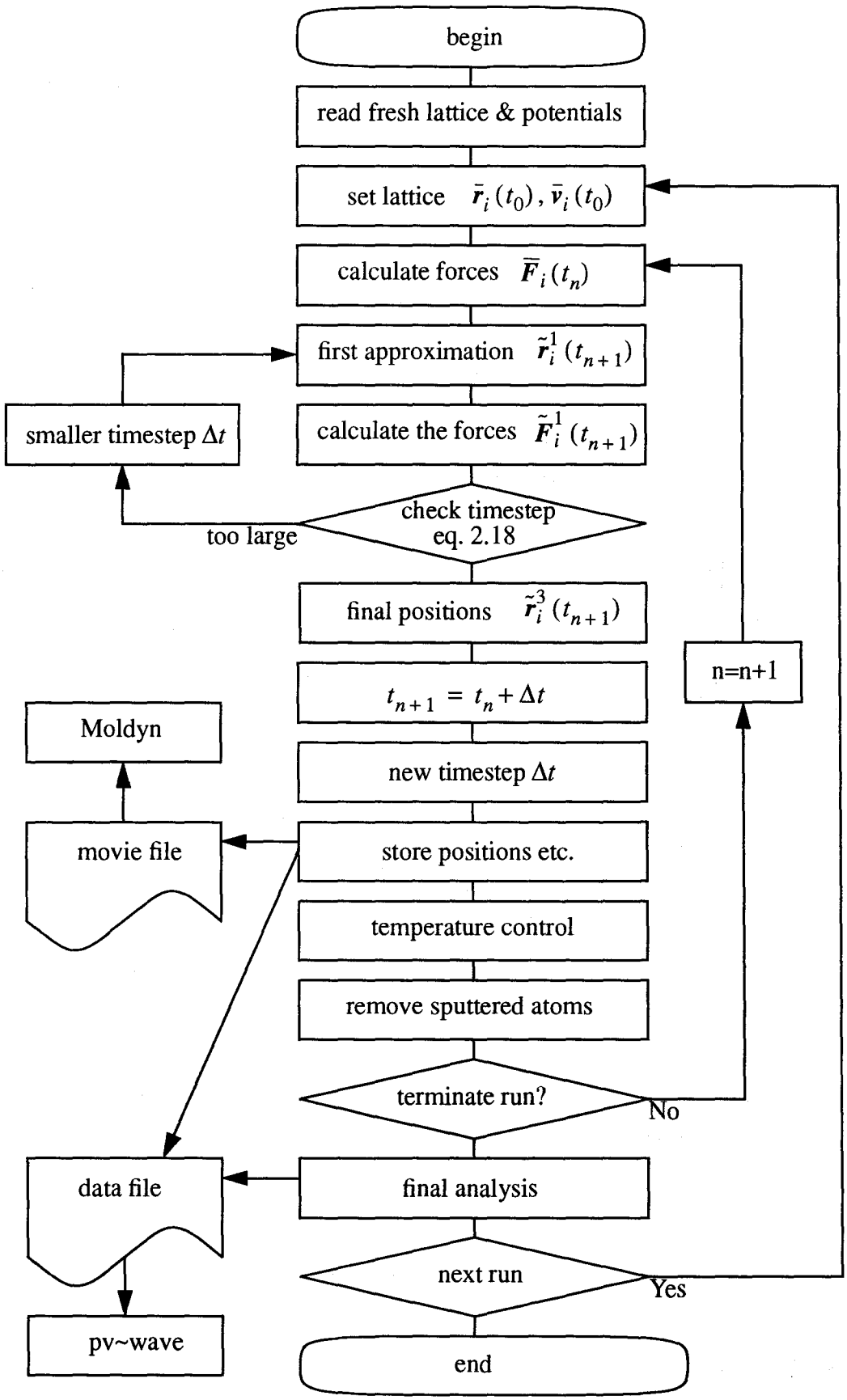

Fig. 2.2 Flowchart of the code. See the text for more details.

available for the interactions between the atoms in these supports, nor for the interactions between the atoms in the support and those in the cluster. Therefore, in the simulations a rhodium support is being used. The errors introduced by this surrogate support are believed to be small, because the timescale of the collision process is much shorter than the timescale of the relaxation effects, see chapter 2.4.4. The support has the bulk rhodium fcc lattice with a lattice constant a of 3.80 Å. The surface has the Miller indices (111). It measures 37.23 Å by 37.61 Å and is three layers thick (4.39 Å), containing a total of 672 atoms. To reduce the boundary effects two different boundary conditions are being used: springs and periodic boundaries conditions.

The atoms in the bottom layer are bound to their lattice positions by springs. The force constant C of these harmonic oscillators was obtained by measuring the curvature of the potential around the equilibrium lattice position. This way a spring constant of about 250 N/m was obtained. A similar force constant was found by measuring the velocity ($\approx$10 km/s) of an acoustic wave propagating through an elongated lattice.

Harmonic oscillators do have a disadvantage: after the impingement of the ion a shockwave arises. Normally this energetic wave would disappear into the bulk and slowly fade away. In the springs, however, the kinetic energy of the wave is converted into potential energy and then back into kinetic energy. In other words, the wave is reflected by the springs. To avoid this reflected wave an algorithm was added to snap the springs. If the velocity at which a bottom atom returns from below to its lattice position exceeds a certain value (depending on the lattice temperature) the spring is turned off (force constant zero). Once the atom is close to its lattice position the spring is turned on again. In the normal (thermal) lattice vibrations the atoms will not exceed this speed limit, these vibrations are undisturbed. In simulations with 2 keV neon this leads to an average energy loss of about 100 eV per run.

If an energetic ion/atom collides with an atom the displacement of the latter can get very large. Atoms in the bottom layer should behave in the same manner, which can only be achieved by completely removing the spring. This is done if the length of the spring exceeds 4.23 Å (the cut-off distance of the rhodium potential). Each thus removed spring is equivalent to an energy loss of about 140 eV. In simulations with 2 keV neon this happens on the average once every three runs.

On the remaining four sides of the support that normally are connected to the bulk periodic boundary conditions are applied. Some care was taken to exclude the fast moving atoms and the freely flying particles from the periodicity. A particle is here defined as an atom or a group of atoms that does not interact (directly nor indirectly) with the support. If a particle approaches the periodic boundaries the periodicity is turned off for the atoms inside this particle, so the particle will drift away from the support. Outside the boundaries the particle is still followed for some time to see whether it is stable or not. This goes on till it has drifted too far away, then its situation is frozen and it is excluded from further timesteps. Something similar is done with particles leaving the support area along the vertical axis. Inside the support fast moving atoms that approach the boundaries are also excluded from periodicity. When the atom passes the boundaries it is entirely removed.

2.4.2 The cluster

The structure and shape of the rhodium clusters is still a subject of research. In transmission electron microscopy (TEM) micrographs all kind of polyhedrons and less regular near spherical shapes can be distinghuished[3]. These 'spherical' shapes are the result of the strong rhodium-rhodium interaction and the weaker rhodium-support interaction.

Filling a polyhedron completely requires a certain number of atoms, 'magic numbers'. A different number of atoms may thus very well lead to another preferential shape, which might explain the wide variety of observed shapes. Remarkable are the results of Iijima and Ichihashi[17]. They observed a gold cluster of about 450 atoms for some time and noticed that the cluster moved, rotated and changed shape approximately every few tenths of a second. Similar results have been found for other fcc metals, including rhodium. They suggested that the electron beam might disturb the cluster, but the raise of the average temperature was estimated to be only roughly 100°C. The energy differences between the various shapes then have to be small to allow for shape/structure transitions.

The results of theoretical studies on the preferential shapes are also not in agreement. In the first prediction by Ino[18] the icosahedron is the favourable shape for clusters up to 40,000 atoms. In later studies all kind of shapes were proposed, ranging from regular structures, like the cuboctahedron and the decahedron, to structures with defects and even glassy shapes[19]. All these shapes have indeed been observed in TEM. The calculated energy differences between the various shapes are very small, of the order of one hundredth of an eV per atom. In these theoretical studies on the shape the influence of the supports is neglected.

For the present simulations a cluster with the frequently observed regular icosahedral shape (a shape with 20 equilateral triangles for its faces) is chosen, see figure 2.3. In the experiments done at the TUE clusters with a diameter of roughly 15 Å were observed[2,6]. An icosahedron of about that size contains 147 atoms. The lattice needed to fill the cluster is not a single continues lattice[20]. If we look at the figures 2.3 and 2.4 we see that the cluster is made of 20 identical pyramids with a triangular basis. The tops of these pyramids lie at the centre of the cluster. Each pyramid can be filled with a rhombohedral (or trigonal) lattice, which is obtained by stretching a fcc lattice along the <111> direction. The top angle then increases from 60° for fcc up to 63.43° ($\text{acos}(1/\sqrt{5})$). Due to the stretching there are two different lattice constants (one in the base-plane of the pyramid and one along the edges), with a ratio of 1.054 ($\sqrt{2-2/\sqrt{5}}$). By combining twenty of these filled pyramids into a single icosahedron the atomic positions are obtained, explaining the name multiply twinned particle.

From a different point of view the cluster has an onion like structure of concentric shells. The centre shell contains a single atom, the surrounding shells contain respectively 12, 42, 92, $10n^2 + 2$ atoms. This shell structure is very prominent visible in the sputter yields. To keep track of the atoms in the calculations they are all marked with a number. In the support the atoms are numbered on a per layer basis. For the atoms in the cluster a special numbering that reflects the original position of the atom was used: they are first sorted by the shell they are in and secondly on their vertical position within the shell.

The cluster was made with one of its lattice constants equal to the bulk lattice constant and then shrunk and expanded around this value till the minimal energy was found. In anneal runs a free cluster appears to be fairly stable, see paragraph 2.4.4. The cluster was

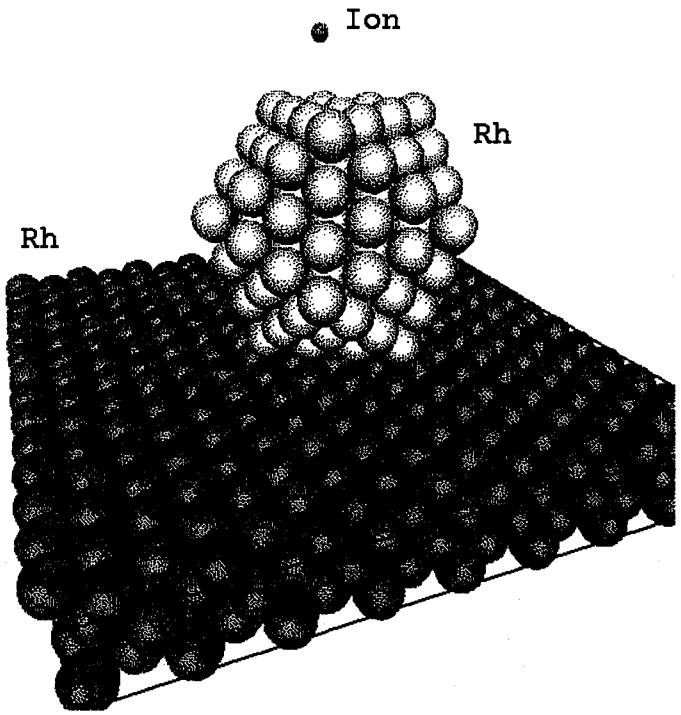

Fig. 2.3 The initial state of a rhodium cluster on top of a rhodium support. The ion is just above the cluster, but out of reach for interactions.

placed on the support with one face parallel to the support surface. Since the surface of the cluster is identical to a fcc - 111 surface (except for the lattice constant) the cluster was rotated and moved until the atoms of the bottom face were at the closed packed positions of the support. From above (figure 2.4) the icosahedron then looks like a hexagon, with sides of 7.59 Å. The length along the x-axis is 15.18 Å, along the y-axis 13.15 Å and the height is 12.28 Å. The cross-section is 149.8 $Å^2$. Anneal runs performed with this cluster-support combination show a slowly deforming cluster (see paragraph 2.4.4), which is expected since rhodium deposited on rhodium tends to wet the surface.

2.4.3 The integrator

The main part of the code is the integrator that solves the equations of motion. To approximate the integral in eq. 2.6 assume that the acceleration is constant between t_0 and t_1. The accelerations at t_0 can simply be calculated with eq. 2.7. Substituting eq. 2.6 into eq. 2.5 gives the first approximation ($^{\sim 1}$) of the positions at t_1:

$$\tilde{\bar{r}}_i^1(t_1) = \bar{r}_i(t_0) + \bar{v}_i(t_0) \cdot \Delta t + \frac{1}{2}\bar{a}_i(t_0) \cdot \Delta t^2. \qquad (2.8)$$

Notice that these are just the first three terms of a Taylor-Maclaurin series expansion of the

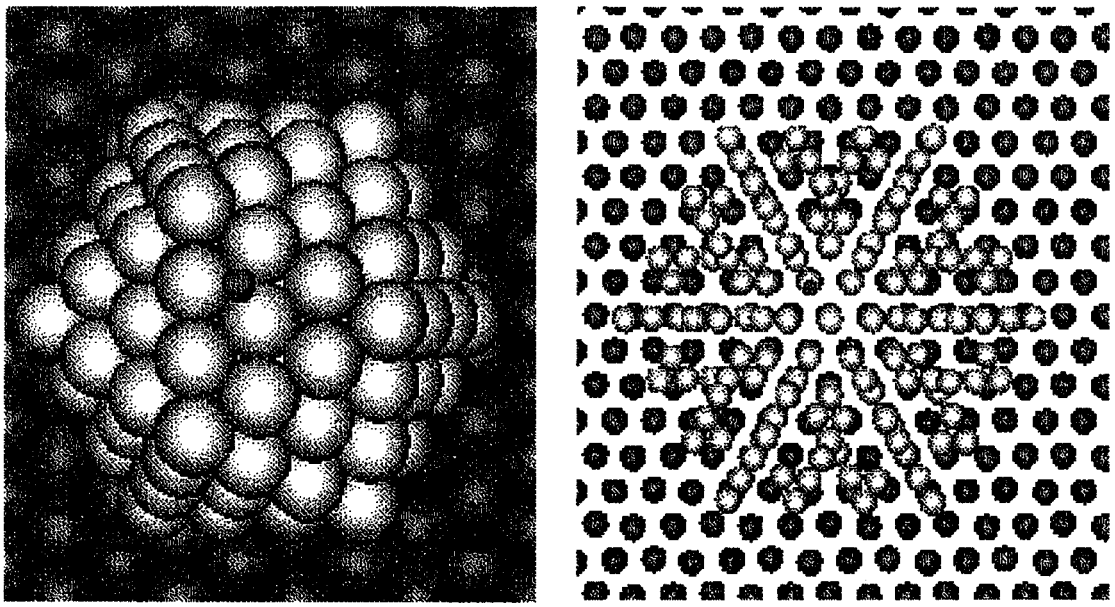

Fig. 2.4 Top view of a cluster on a support. On the left the spheres represent the electron clouds of the atoms. On the right the smaller spheres represent the scattering areas.

position with respect to time. The error (^) made by assuming a constant acceleration is

$$\hat{\boldsymbol{r}}_i^1(t_1) = \frac{\Delta t^3}{6} \cdot \frac{d}{dt}\bar{\boldsymbol{a}}_i(\xi) \qquad t_0 \le \xi \le t_1, \tag{2.9}$$

which is the rest term of Lagrange. By doubling the timestep the error increases by a factor of about eight, the method is of third order accuracy. For the velocity we may use

$$\tilde{\boldsymbol{v}}_i^1(t_1) = \bar{\boldsymbol{v}}_i(t_0) + \bar{\boldsymbol{a}}_i(t_0) \cdot \Delta t, \tag{2.10}$$

which is of second order. We now have derived a set of positions and velocities for time t_1. In other words: we have arrived at a situation like before eq. 2.8, but time has advanced by Δt. This is an iterative process. To describe the entire collision process this procedure is repeated typically of the order of a thousand times. Note that the newly calculated positions and velocities may very well differ from their exact values. Since these new values are being used as the input for the next step the errors will tend to increase in each step.

In the next step the positions $\tilde{\boldsymbol{r}}_i^1(t_1)$ are substituted into eq. 2.7 to get the accelerations $\tilde{\boldsymbol{a}}_i^1(t_1)$. These are needed in the calculation of $\tilde{\boldsymbol{r}}_i^1(t_2)$, but they can also be used to decrease the error in the determination of the velocity, when applied in

$$\tilde{\boldsymbol{v}}_i^2(t_1) = \bar{\boldsymbol{v}}_i(t_0) + [\bar{\boldsymbol{a}}_i(t_0) + \tilde{\boldsymbol{a}}_i^1(t_1)] \cdot \frac{\Delta t}{2}. \tag{2.11}$$

The velocities now are of third order, using only a minimum of extra computer time. The combination of eq. 2.8 and 2.11 is known as the velocity form of the Verlet algorithm[21].

A more accurate algorithm for the positions is the average force method of Harrison *et al.*[22]. The positions are calculated by

$$\tilde{\bar{r}}_i^2(t_1) = \bar{r}_i(t_0) + \bar{v}_i(t_0) \cdot \Delta t + [\bar{a}_i(t_0) + \tilde{\bar{a}}_i^1(t_1)] \cdot \frac{\Delta t^2}{4}. \qquad (2.12)$$

The idea is that this averaged acceleration is closer to the actual time averaged acceleration during the timestep than the acceleration at the beginning of the timestep. The error in the position now is

$$\hat{\bar{r}}_i^2(t_1) = \frac{\Delta t^3}{12} \cdot \frac{d}{dt}\bar{a}_i(\xi) \qquad t_0 \le \xi \le t_1. \qquad (2.13)$$

If we compare this with eq. 2.9 this new method is only better by a factor of two. However, including the acceleration at t_1 makes it theoretically possible to improve the accurateness by one order. Smith and Harrison[23] showed that with better chosen weighting coefficients the average force method grows to full advantage. In

$$\tilde{\bar{r}}_i^3(t_1) = \bar{r}_i(t_0) + \bar{v}_i(t_0) \cdot \Delta t + [2\bar{a}_i(t_0) + \tilde{\bar{a}}_i^1(t_1)] \cdot \frac{\Delta t^2}{6} \qquad (2.14)$$

the error is as low as

$$\hat{\bar{r}}_i^3(t_1) = \frac{\Delta t^4}{24} \cdot \frac{\partial^2}{\partial t^2}\bar{a}_i(\xi) \qquad t_0 \le \xi \le t_1. \qquad (2.15)$$

This is indeed a fourth order method. The difference between eq. 2.13 and 2.15 looks impressive, but in reality it turns out to be only very small. The average force method is a so-called predictor-corrector method: first $\bar{r}_i(t_1)$ is approximate and then that value is used to close in on the actual value.

In comparison with the Verlet method the number of calculations per timestep has doubled and in return the error was reduced. It is worth it to put in the extra computation time, since due to the smaller error a larger timestep can be afforded. If the timestep in eq. 2.14 is twice the timestep used in eq. 2.8 (so both methods have the same number of calculations per time interval) the error in eq. 2.15 is equal to, or less than, the error in eq. 2.9[22]. This justifies the use of the average force method.

In molecular dynamics simulations where the velocities of the particles are in a narrow range (like when simulating a liquid) a constant timestep is very common. For energetic ion bombardment, however, a variable timestep is more appropriate. In the first part of the simulation the fast moving ion undergoes one or more hard collisions. To describe these accurately the timestep must be fairly small, of the order of 0.1 fs. In the later steps a lot of kinetic energy has been dissipated by the escaped atoms and/or ion. Since these do not interact any more with the cluster nor the support, they are excluded in the determination of the timestep. The remaining atoms do have small velocities and their interactions are weak, permitting a larger timestep up to 10 fs. The above discussed integrator algorithms have the advantage that it is fairly simple to vary the timestep during the simulation.

For the determination of the timestep we return to eq. 2.8. For accurate calculations this truncated series must converge rapidly, so

$$\bar{v}_i(t_0) \gg \frac{1}{2}\bar{a}_i(t_0) \cdot \Delta t. \qquad (2.16)$$

We then find

$$\Delta t \approx \frac{\left|\tilde{\bar{r}}_i^1(t_1) - \bar{r}_i(t_0)\right|}{\left|\bar{v}_i(t_0)\right|}. \qquad (2.17)$$

A reasonable timestep is therefore obtained by the choice of an acceptable maximum displacement per timestep Δr_{max} and dividing this distance by the velocity of the fastest atom. In the simulations a value of 0.04 Å was used.

Another good timestep indicator is the error in the newly calculated positions. Notice that

$$[\tilde{\bar{F}}_i^1(t_1) - \bar{F}_i(t_0)] \cdot \frac{\Delta t^2}{2m_i} = \tilde{\bar{r}}_i^2(t_1) - \tilde{\bar{r}}_i^1(t_1) \approx \frac{\partial}{\partial t}\bar{a}_i(\zeta) \cdot \frac{\Delta t^3}{2} \qquad t_0 \le \zeta \le t_1. \quad (2.18)$$

In other words: the difference between the two calculated positions (or forces) is closely related to the error in the position as given by eq. 2.13. This relation can be used in two different ways:

i to check during a cycle whether the current timestep is not too large. An upperlimit (in this case 10^{-3}Å) can be used on the permitted error in the position. If an error exceeds this limit, the timestep is reduced and re-substituted into eq. 2.8 and following.

ii to determine a new timestep for the next cycle. With a method similar to the one discussed above the maximum permitted timestep is calculated. This timestep is then combined with the current timestep and the one obtained from eq. 2.17 to find a new timestep for the next iteration step.

During the run we keep track of the atoms that escape upwards, downwards or sidewards. Usually these are the fastest moving atoms, responsible for the small timestep. As soon as they are away far enough from the support/cluster they are excluded from the timestep algorithm. At even larger distances they are excluded from the integrator, since they are not likely to interact any more. In the time period between these two situations their positions are still calculated, to see whether the formed multimers are stable.

A run can be terminated when all atoms on/in the support have a low potential energy and/or velocity, indicating that they are close to a stable situation. Another method is to stop the run after a fixed number of timesteps. After examining the movies of several collisions a number of 2,500 steps was chosen. Because of the variable timestep this does not impose a limit on the elapsed time. It varies between 1 and 8 picosecond.

The integrator algorithm is not perfect, since the set of eq. 2.5,2.6 and 2.7 is not solved exactly but approximated. As a result the positions, velocities and energy of the atoms contain small errors. The simplest error to calculate is the difference between the total energy (at a certain point in time) and the initial value of the total energy. There are no inelastic collisions and the energy losses due to temperature control (see 2.4.4) and snapping springs can be corrected for. The maximum error in the total energy throughout a run is nearly always less than 15 eV. As a comparison, initially the potential energy is -4.3 keV and all kinetic energy is contained in the ion.

2.4.4 Temperature control

Initially all atoms, except the ion, are at their lattice positions with zero velocity. The potential energy is then close to its minimum and all kinetic energy is stored in the ion. In a series of collisions this kinetic energy is distributed over all atoms in the cluster and the support. This will cause a severe distortion of the area around the impact point. Normally this energy would be distributed over an increasing number of atoms. However, in the simulation this will not happen since the number of atoms is limited. Part of the energy loss to the bulk is already incorporated by the snapping springs in the bottom layer and by the atoms that leave the support downwards. An additional energy loss is obtained by simulating the thermal coupling of the support to an external bath of constant temperature T_0=300 K. According to Berendsen *et al.*[24] this can be done by multiplying the velocities of selected atoms after each timestep by

$$\lambda = \sqrt{1 + \frac{\Delta t}{\tau}\left(\frac{T_0}{T} - 1\right)}, \tag{2.19}$$

where T is the average temperature of the selected atoms, τ a timeconstant (in our case 400 fs) and Δt the timestep. This multiplication factor λ is applied on all support atoms below the surface layer. In simulations with 2 keV neon this results in an average loss of about 45 eV per run.

To determine if temperature affects the structure of the support and the cluster some anneal runs were done. In these runs the atoms start at their lattice positions with a randomly orientated velocity $v_i(t_0) = \sqrt{k_B T_1 / m_i}$. The ion is absent. In this manner the stability of the cluster and/or support was tested. A parameter for the order in the lattice is the so-called pair distribution function,

$$g(r) = \sum_{i>j}^{N} \delta(|\boldsymbol{r}_i - \boldsymbol{r}_j|), \tag{2.20}$$

which counts the pairs of atoms a distance r apart. Figure 2.5 shows this distribution for a free cluster at three situations. For the fresh cluster two peaks are prominent, they correspond with the two lattice constants. During an anneal run at 300 K for 17 ps the peaks broaden but they do not shift. In the second run the cluster was first thoroughly shaken at 300 K and then cooled down to 1 K in 31 ps with a timeconstant τ of 10 ps. In the final situation the sharp peaks of the initial situation reappear.

In anneal runs of a cluster on top of the support at 300 K for 24 ps the cluster preserves its shape. At higher temperatures (600 K) the cluster lowers, the contact area between cluster and support increases, but the atoms remain together. Not till temperatures over 1200 K the cluster starts spreading out, and some atoms diffuse over the support. This happens on a timescale of 10 ps. From these data we conclude that the cluster on top of the support is in a local minimum of potential energy. The cluster recovers from small perturbations, but with larger disturbances (high temperatures, impinging ions) the cluster will decay.

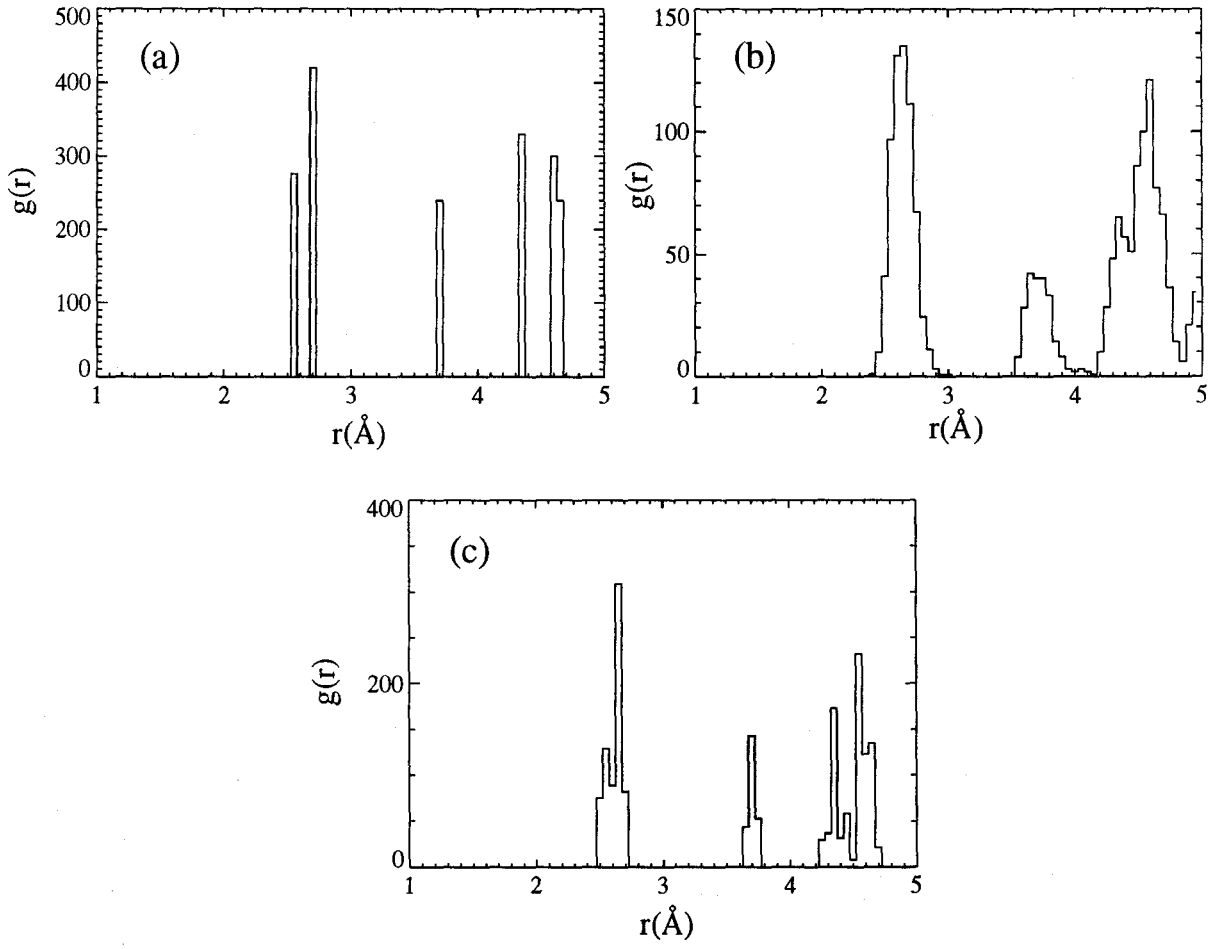

Fig. 2.5 The pair distribution function for the icosahedral cluster, a) initial situation, b) annealed at 300 K and c) cooled from 300 K down to 1 K.

2.4.5 Analysis

During the course of the program several data are stored in files for analysis:

- During the run the atomic positions can be stored every couple of timesteps. This list of positions can then be visualized by the program 'moldyn' as a movie of the collision process. Figures 2.3, 2.4 and 3.1 were made this way.
- At the end of the run all information on the final situation is stored for possible future use. It is for instance possible to use the final situation as a starting point for following runs.
- A part of the code was written to sort out the atoms in the final situation. This is done by an algorithm that groups all atoms and determines the position and velocity of their centre of mass. The most interesting groups are those that are freely flying above the support, since these are the ones that are measured in a LEIS or

SIMS experiment. A similar algorithm is applied on the atoms that originate from the cluster, to see how many of them ended up on top of or in the support. Both these collections of groups are stored in files. These files are then read and analysed by 'pv~wave', visual data analysis software.

2.5 The interaction potential.

The rhodium-rhodium interactions are described by a many body potential, the so-called Embedded Atom Method (EAM), as proposed by Daw and Baskes[25]. The idea is that the potential energy of atom i, surrounded by neighbours, is given by

$$E_i = F_i(\rho_i) + \frac{1}{2}\sum_{j \neq i} \phi_{ij}(r_{ij}) . \tag{2.21}$$

In the nuclear repulsion $\phi(r)$ we recognize a linear part, the core-core repulsion, just like for two body potentials. In addition there is a non linear part, the embedding function $F(\rho)$. This term gives the energy of an atom embedded in the electron gas caused by surrounding atoms. Suppose that this background electron density is approximated by a superposition of the free atomic densities ρ_j^a of the neighbouring atoms, then

$$\rho_i = \sum_{j \neq i} \rho_j^a(|\boldsymbol{r}_i - \boldsymbol{r}_j|) . \tag{2.22}$$

This is of course only valid if the covalent bonds are small, like for instance in simple metals and metals with nearly filled outer shells. In eq. 2.22 it is also assumed that the atomic electron densities are spherical symmetrical. A thorough derivation of the EAM, based on density functional theory, was given by Daw[26]. He also showed that small electron redistributions (due to bonds) do not change the form of the equations. As Baskes *et al.*[27] showed, the EAM can also be used for covalent bound silicon by introducing an angle dependence in the atomic electron density.

The main problem is to determine the functions F, ρ^a and ϕ. There are two ways of doing this. In the first place the energy versus electron-density relations obtained in density functional theory may be used. This has been done for nickel, leaving only two fitting parameters[26], one on the electron distribution in the outer shells and one on the mobility of the electrons. Nevertheless, the predictions of various bulk properties are in reasonable agreement with experimental data.

We however use the method by Foiles *et al.*[28], in which the functions are obtained by fitting them to experimental data. Because of this preparation method the results probably are in closer agreement with experiments. First a monotone decaying (and thus invertible) atomic electron density is chosen,

$$\rho^a(r) = \begin{cases} \text{Linear with negative slope} & r \leq 0.56 \text{ Å} \\ \rho_{scf}(r) & 0.56 \text{ Å} \leq r \leq 4.23 \text{ Å} \\ 0 & r \geq 4.23 \text{ Å} \end{cases} , \tag{2.23}$$

where $\rho_{scf}(r)$ is a spherically averaged self-consistent field density function[29]. This density is shown in figure 2.6. Since the lattice of rhodium is known to be fcc, the background

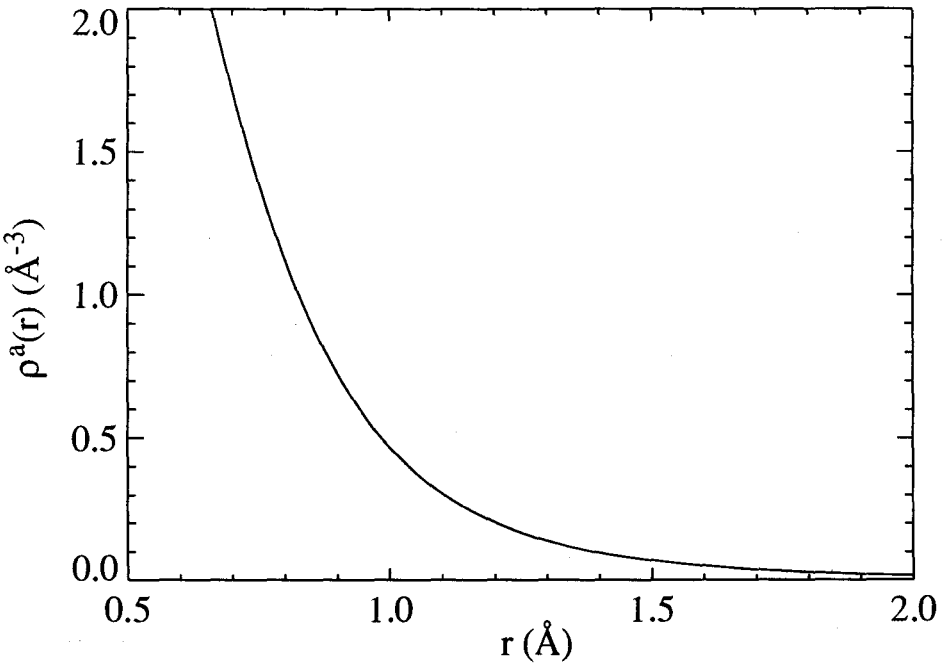

Fig. 2.6 Electron density of a free atom as a function of distance to the nucleus.

electron density at atom i is

$$\underline{\rho}_i(a) = \sum_{m=1}^{n} \rho^a[r_m(a)], \tag{2.24}$$

where a denotes the lattice constant and r_m the position of the m^{th} neighbour. To avoid confusion the underscore (_) is used to mark summed values. The number of neighbours n must be large enough to include all neighbours within the cut-off distance. For lattices uniformly compressed or expanded by less than 10% the energy per atom is described by the universal scaling relation of Rose *et al.*[30],

$$E_{Rose}(a) = -E_s(1+a^*)e^{-a^*}, \tag{2.25}$$

where a^* is a measure of the deviation from equilibrium,

$$a^* = (\frac{a}{a_0} - 1)\sqrt{\frac{9B\Omega}{E_s}}. \tag{2.26}$$

The introduced bulk parameters are the equilibrium sublimation energy E_s, the bulk modulus B, the equilibrium lattice constant a_0 and the equilibrium volume per atom Ω. The nuclear repulsion function is chosen as

$$\phi(r) = \frac{Z^2(r)\,e^2}{4\pi\varepsilon_0 r}, \tag{2.27}$$

where

$$Z(r) = Z_0(1+\varepsilon r^{\upsilon})\,e^{-\alpha r}. \tag{2.28}$$

The value of Z_0 will be assumed to be given by the number of outer electrons of the rhodium atom, so Z_0=9. Similar to eq. 2.24 a summed nuclear repulsion $\underline{\phi}_i(a)$ is defined. Combining eq. 2.21 and 2.25 the embedding function is

$$F[\underline{\rho}_i(a)] = E_{Rose}(a) - \frac{1}{2}\underline{\phi}_i(a). \tag{2.29}$$

This function still depends on the choice of α, ε and υ. Substituting eq. 2.27 and 2.29 into eq. 2.21 the energies of various distorted lattices can be calculated as a function of these three parameters. They were fitted on the elastic constants c_{11}, c_{44} and the vacancy formation energy E_v of bulk rhodium. The potential now is suitable for describing lattice like situations, and does indeed correctly predict various bulk parameters[28].

During ion bombardment the interatomic distances may get much larger and/or smaller than in a normal lattice. For these situations the EAM potential is not yet adequate. For small interatomic distances a screened Coulomb potential is common used,

$$V_{ij}(r) = \frac{Z_i Z_j e^2}{4\pi\varepsilon_0 r}\phi\left(\frac{r}{a_s}\right). \tag{2.30}$$

In the Molière potential[31] the screening function is

$$\phi\left(\frac{r}{a_s}\right) = 0.35\cdot exp\left(-0.3\frac{r}{a_s}\right) + 0.55\cdot exp\left(-1.2\frac{r}{a_s}\right) + 0.10\cdot exp\left(-6.0\frac{r}{a_s}\right). \tag{2.31}$$

The screening length a_s depends on the charges,

$$a_s = \left(\frac{9\pi^2}{128}\right)^{1/3} a_{Bohr}\left(Z_i^x + Z_j^x\right)^{-y/3}, \tag{2.32}$$

where a_{Bohr} is the Bohr radius (≈0.529 Å). The coefficients x=1/2 and y=2 were proposed by Firsov[32]. A smooth transition from the EAM to the Molière potential was obtained by making $F_i(\rho)$ linear for densities higher than $\underline{\rho}_i(0.9a_0)$ [10]. The embedding function then looks like figure 2.7. By making this non-linear part of eq. 2.21 linear, the relation reduces to two sums over all atom-pairs including atom i, just like used for two body potentials. To obtain the correct two body potential the nuclear repulsion function is changed into,

$$\phi(r) = V_{Moliere}(r) - 2F[\rho_i^a(r)]. \tag{2.33}$$

This function is shown in figure 2.8.

For the large interatomic distances, electron background densities less than $\underline{\rho}_i(1.1a_0)$, a smooth transition is made to the Morse potential[33],

$$V(r) = D\cdot e^{-2\alpha(r-r_0)} - 2D\cdot e^{-\alpha(r-r_0)}. \tag{2.34}$$

This potential is often used to describe dimers, where the binding state is at a distance r_0

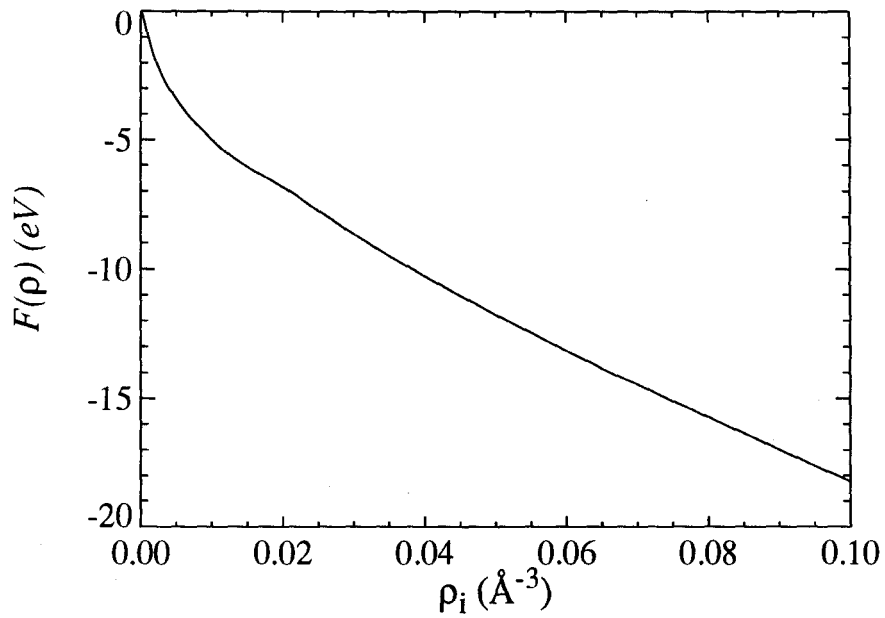

Fig. 2.7 The embedding function versus the background electron density. The lattice-like ρ_i *ranges from* $1.8 \cdot 10^{-2}$ *till* $6.9 \cdot 10^{-2}$ *Å*$^{-3}$.

and with bindings energy D. The factor α determines the curvature of the potential and thus the vibration spectrum. This potential is added to describe the interactions in sputtered rhodium dimers. If the nuclear repulsion function of eq. 2.28 is used, the embedding function has the form

$$F[\rho_i^a(r)] = \frac{1}{2}[V_{Morse}(r) - \phi(r)]. \tag{2.35}$$

The functions Z and F were smoothed by splines at the various intersection points. This potential was developed and used by Garrison *et al.*[10] for the simulation of sputtering from bulk rhodium.

In computations the potentials are cut off for large (couple of angstrom) interatomic distances, because the interactions then become very weak. If the potential suddenly drops to zero its derivative (the force) contains a delta function. This can be avoided by smoothing the transition to zero at the cut-off distance r_c. The above mentioned Morse and Molière potentials are therefore multiplied by the Tersoff cut-off function[34]

$$F(r) = \begin{cases} 1 & r \le r_c - 2\delta \\ \frac{1}{2}\left[1 - \sin\left(\pi\frac{r - r_c - \delta}{2\delta}\right)\right], & \text{for } r_c - 2\delta \le r \le r_c \\ 0 & r \ge r_c \end{cases}. \tag{2.36}$$

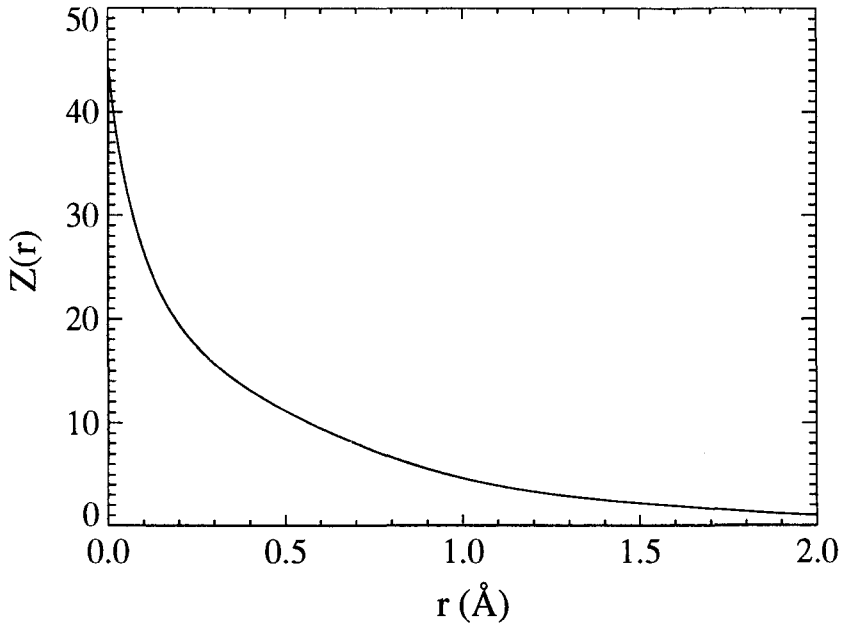

Fig. 2.8 The nuclear repulsion function versus the interatomic distance.

This makes sure that between $r_c - 2\delta$ and r_c the potential is smoothly turned off. In the rhodium potential the Morse potential was multiplied by this cut-off function, with an r_c of 4.23 Å and a δ of 0.772 Å. The ion-rhodium interaction is described by the product of the Molière potential and the Tersoff function, turned off at 3.23 Å. Noble gas ions are inert, so their interaction potential does not require a minimum.

Each time the forces and the energies of the atoms are determined all interatomic distances must be calculated. Most of them (they number $N(N-1)/2$) are larger than the cut-off distance r_c of the potential, so calculating them over and over again is a waist of time. Computer time can be saved by using a neighbour list. In this list all couples whose separation is less than $r_{nl} = r_c + 2r_d + r_{sm}$ are stored. The average number of neighbours per atom is about 25, so the list contains about $25N/2$ couples. If an atom has moved more than r_d (a value of 0.3 Å was used) since the last neighbour list was made a new list becomes necessary. Making this list of course requires calculating the distances between all possible atom-pairs. For safety reasons a safety margin r_{sm} was added.

Each timestep the potential energies and the forces are calculated twice. This takes quite a lot of time, especially for the more complicated potential functions like used in the EAM. To save time, at the beginning of a (series of) iteration run(s) the potentials and forces are either calculated or read from a file and then stored in an array. During the run potentials are obtained by a linear interpolation between points in this array.

3 Results

3.1 Introduction

With the previously discussed code and potentials some 2900 ion trajectories were calculated, using helium-4, neon and argon with energies in the range 0.5 - 5 keV. Before analysing the information it is enlightening to take a look at a scattering process, as will be done in the next paragraph. This clarifies the distinction made between atoms sputtered upwards and those sputtered downwards. It also shows how destructive ion scattering is, though the idea of an exploding cluster turns out to be an overestimation.

3.2 A scattering process

To give an impression of what goes on when an ion is scattered on a cluster a particular scattering run is shown in detail. In this run a 2 keV neon ion is scattered on the centre atom in the top surface of the cluster. An impact parameter of 0.071 Å was chosen, so the ion is scattered over 145° and leaves the region after only one collision. This is the kind of event that can be detected in the EARISS[8], provided the ion has not neutralized. At time $t=0$ the ion is at 1.1 times the cut-off distance r_c above the cluster, like depicted in figure 2.3. In the hard collision the ion loses 40% of its kinetic energy and is deflected, never to return. In this collision process the neon and the rhodium atom interact during no more than 7 fs. The interaction force gets as high as 100 micro Newton. Figure 3.1 shows the process at various points in time. The top central atom loses its surplus of energy (800 eV) by setting other atoms in motion, resulting in an increasing number of moving atoms with decreasing energy. Eventually also some energy is passed on to the support. Various atoms gain enough energy to escape from the cluster, several of these are marked in the pictures by arrows. Some are going upwards, these are the ones that are detected in a SIMS experiment. Others are going downwards and will after some time adsorb on the support surface, or sometimes even penetrate into the support. In several runs they were observed to re-unit with the cluster. If a following ion impinges near this cluster it might be scattered on these downwards sputtered atoms. Calculating this scattering process took half an hour.

In the above visualized scattering process the ion loses about half its energy in a single collision and then disappears. The cluster is severely damaged. This kind of process is typical for high energetic heavy ions. With a light helium ion however, the damaging process looks quite different. Because of its low mass helium can lose only a relatively small part of its energy per collision, a maximum of 14.4% versus 54.8% for neon and 80.6% for argon. As a result the helium ion scatters around through the cluster, resembling a pin-ball machine. The sputtering results mainly from primary recoils (primary knock on) instead of recoil atoms generated in a collision cascade (secondary knock on). On the average helium ions cause less damage than the heavier ions, but they are capable of afflicting serious damage to a cluster.

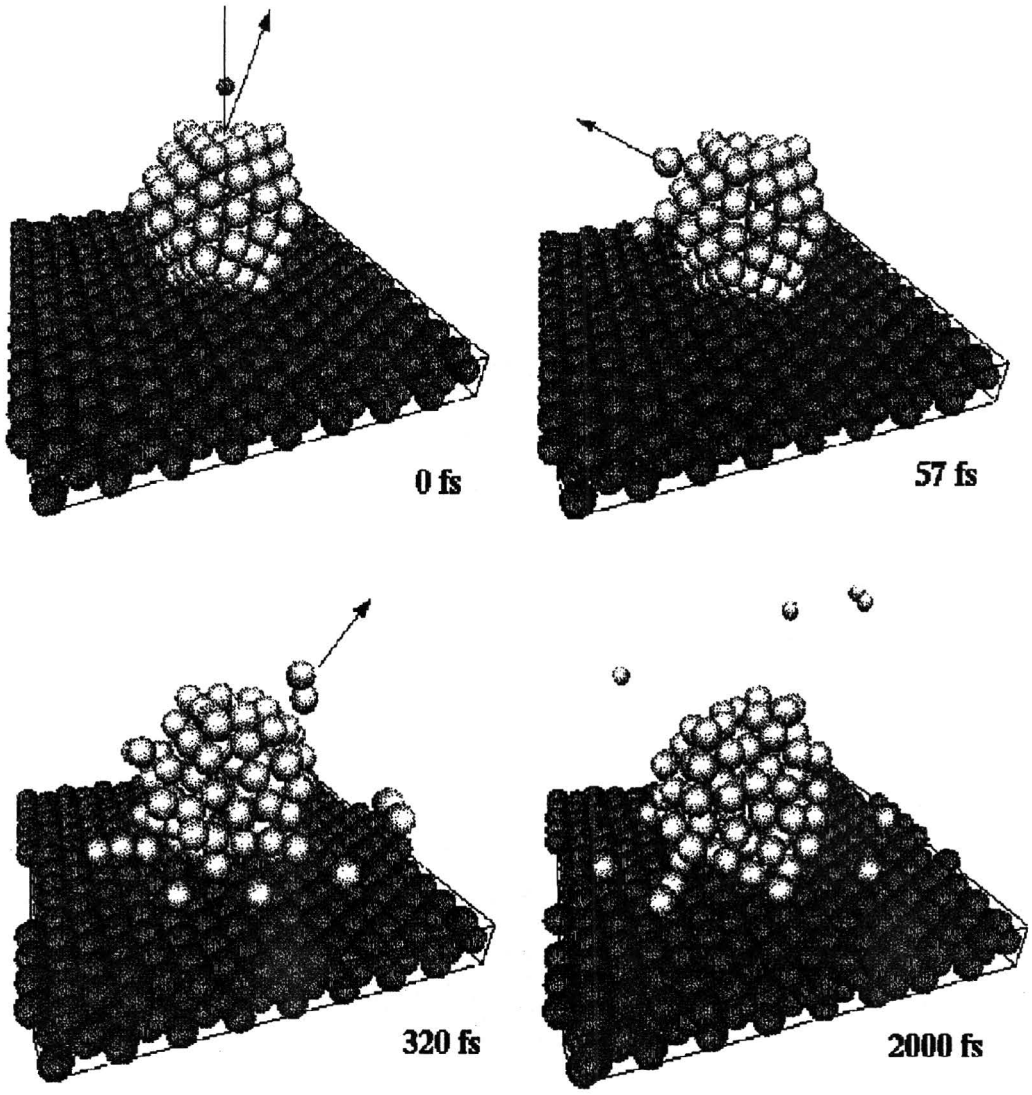

Fig. 3.1 A 2 keV neon ion is scattered over 145 ° from the centre atom of the top surface of the cluster. A total of 9 atoms is sputtered upwards and 5 landed on the support.

3.3 Sputter yields

In LEIS and SIMS experiments the position at which an ion impinges on the sample is not known, because the diameter of the ion beam (the order of a mm) is much larger than that of a cluster. This is simulated by a distribution of the impact points of the vertically incoming ions over the cluster and part of the neighbouring support. As the topview in figure 2.4 shows the cluster and support do have a six-fold symmetry, so only one sixth of the cluster needs to be sampled. Usually, a set of impact points is obtained by uniform sampling of a representative area. We however used a random distribution of impact points. Over-

sampling the points of high symmetry (that may give raise to unrealistic sputter yields) is thus avoided. The equilateral triangle of random impact points has a height of 12 Å, with the top lying at the centre of the cluster. Three impact areas can be distinguished:

i One third of the ions impinges within the outer boundaries of the cluster. These are likely to damage the cluster.

ii Another one third of the ions comes within the cut off distance (for the ion-rhodium interaction 3.23Å) of the cluster. The ions that are close to the cluster will probably damage the cluster, while the more distant impinging ions have hardly any direct influence on the cluster. There is, however, no sharp border between these two regions. In the following analysis the areas *i* and *ii* are combined.

iii The remaining one third of the ions does not interact with the cluster before reaching the support. They may still damage the cluster though, by means of the shock wave or energetic sputtered atoms. Since the support is only three layers thick the collision cascade can not develop completely. The sputter yields in this area therefore are merely an indication of the bulk sputter yields.

In the simulations three different ions were used: helium-4, neon and argon. Their initial kinetic energies were 0.5, 2.0 and 5.0 keV. For each possible ion and energy combination 200 trajectories were performed, each using the same list of impact points. The analysis on the damage of cluster and support are given in table 3.1. We see that, as expected, the

Table 3.1: Average sputter yields per incident ion.
See also the tables in the appendix.

ion, energy	Atoms sputtered upwards from cluster. Areas *i* & *ii*	Atoms sputtered downwards from cluster. Areas *i* & *ii*	Atoms sputtered upwards from support. Areas *i* & *ii*	Atoms sputtered upwards from support. Area *iii*	Percentage of returned ions. Areas *i* & *ii*
He, 0.5 keV	0.06	0.12	0.02	0.10	27
He, 2.0 keV	0.09	0.18	0.04	0.01	5
He, 5.0 keV	0.16	0.20	0.07	0.01	5
Ne, 0.5 keV	1.3	1.2	0.5	0.8	50
Ne, 2.0 keV	2.3	1.7	0.9	1.0	23
Ne, 5.0 keV	1.7	1.5	0.8	0.6	15
Ar, 0.5 keV	1.9	2.0	0.7	1.0	64
Ar, 2.0 keV	4.4	3.9	2.2	2.1	37
Ar, 5.0 keV	3.8	3.1	2.1	1.2	20

number of atoms sputtered upwards from the clusters is considerably higher than the number sputtered upwards from the support. This difference is due to the geometry of the cluster. If a collision cascade develops in the cluster it will quickly reach the surface and sputter atoms. In the support this is more difficult. The bindings energy of the atoms in the outer shell of the cluster is 4.9 eV, hardly less than the 5.1 eV of the atoms in the surface of the support.

With increasing ion mass the number of sputtered atoms increases, because a heavier ion can deposit more energy per collision. At the same time the scattering impact parameters for neon and argon are about twice those for helium, see table 3.2, giving the heavy ions

Table 3.2: Impact parameters for the scattering of an ion on rhodium over an angle of θ.

Ion, energy	$b(\theta=145°)$ Å	$db(\theta=145°)/d\theta$ 10^{-3}Å/°	$b(\theta=90°)$ Å
He, 0.5 keV	0.0757	2.3	0.221
He, 2.0 keV	0.0367	1.1	0.109
He, 5.0 keV	0.0210	0.6	0.064
Ne, 0.5 keV	0.1277	3.8	0.375
Ne, 2.0 keV	0.0710	2.1	0.213
Ne, 5.0 keV	0.0453	1.4	0.137
Ar, 0.5 keV	0.1216	3.7	0.382
Ar, 2.0 keV	0.0732	2.3	0.234
Ar, 5.0 keV	0.0486	1.5	0.157

a four times higher chance to scatter, and thus to deposit their energy.

For neon and argon all sputter yields first increase with increasing kinetic energy and then decrease. This profile is also seen in the sputtering of polycrystalline samples[35], where the maximum lies at a somewhat higher energy. For helium the sputter yields do not go down, probably the maximum lies close to 5 keV.

The number of backscattered ions decreases with increasing kinetic energy, because the scattering cross section decreases with increasing energy, see table 3.2. This effect also explains why the number of backscattered ions increases with increasing ion mass. Most of the backscattered ions went through more than one collision, a very small fraction of the backscattered ions has been scattered only once. To get an impression: for a 2 keV neon to be backscattered on a rhodium atom it must impinge within an area of $\pi b^2\,(\theta = 90°) \approx 0.143 Å^2$. That is only 2.3% of the area occupied by a rhodium atom in the (111) surface (6.27 $Å^2$). In the EARISS only ions backscattered over 145° are measured.

This signal is proportional to the area A of a ring around the scattering rhodium atom from which ions are scattered in this direction,

$$A = 2\pi b(\theta = 145°)\frac{d}{d\theta}b(\theta = 145°)\Delta\theta, \tag{3.1}$$

where $\Delta\theta$ is the aperture of the detector. The impact parameter and its derivative are given in table 3.2. The area is the largest when using neon at 0.5 keV. The ratio of the area and the inflicted damage is best for helium at 0.5 keV. These results may drastically change when the neutralization chance of the ion is also taken into account.

There are more atoms sputtered upwards than downwards. Conservation of momentum suggests that the majority of atoms goes downwards, but that direction is blocked by the underlying layers and the support. For helium the majority of the sputtered atoms goes downwards.

The number of sputtered support atoms in the combined areas *i* and *ii* is remarkably high. This could be the result of ions that are deflected by the cluster before they impinge on the support. With increasing angle of incidence the sputter yields are known to increase[36].

The sputter yields for the support are in reasonable agreement with those for polycrystalline rhodium[35] and palladium[36]: about 0.1 for helium, 1 for neon and 2 for argon. At 5 keV the experimental values still go up slowly, while the calculated ones already decrease. This could be an artefact of the comparison with polycrystalline measurements, which might differ from the crystalline yields as was observed for copper[36].

With neon additional runs at the intermediate energies 1, 3 and 4 keV were performed. The results from these runs confirm the above mentioned energy dependencies.

To get better statistics 500 extra runs were done with 2 keV neon. Since ions impinging at more than r_c besides the cluster hardly ever damage the cluster the impact area was reduced to the areas *i* and *ii*, as to increase the frequency of sputtering. Some statistics on these runs are shown in table 3.3. In this table a cluster or support is considered damaged if at least one atom has been removed. This happens for nearly 90% of the ions impinging in area *i*. For argon this figure is a little bit higher, but for helium it is only 25%. The ions impinging in area *ii* are not efficient in destroying the cluster. Argon gives a slightly higher percentage of 20, while for helium it is as low as 2%. Of the atoms sputtered upwards from the cluster 55% is single, 29% is a dimer and 9% a trimer.

3.4 Distributions

In a SIMS experiment the various distributions of the upwards sputtered atoms are analysed. A common selection of the detected atoms is by mass, as to distinguish between (Rh) atoms sputtered from the cluster and (Al,Si,O) atoms sputtered from the support. Another selection that is often made is by the kinetic energy of the sputtered atoms. The extended simulations with 2 keV neon show a kinetic energy distribution as depicted in figure 3.2. In this plot only upwards flying single rhodium atoms (originating from the cluster) are counted. Atoms sputtered from a bulk sample have a kinetic energy distribution of the form[9]

Table 3.3: Extended run with 2 keV neon. Expectation values per incident ion.

	Area *i*	Area *ii*
Atoms sputtered upwards from cluster	3.38	0.36
Atoms sputtered downwards from cluster	2.95	0.21
Atoms sputtered upwards from support	0.90	1.17
Percentage of clusters that is damaged	88	14
Percentage of supports that is damaged	43	54
Percentage of ions that returns upwards	23	23

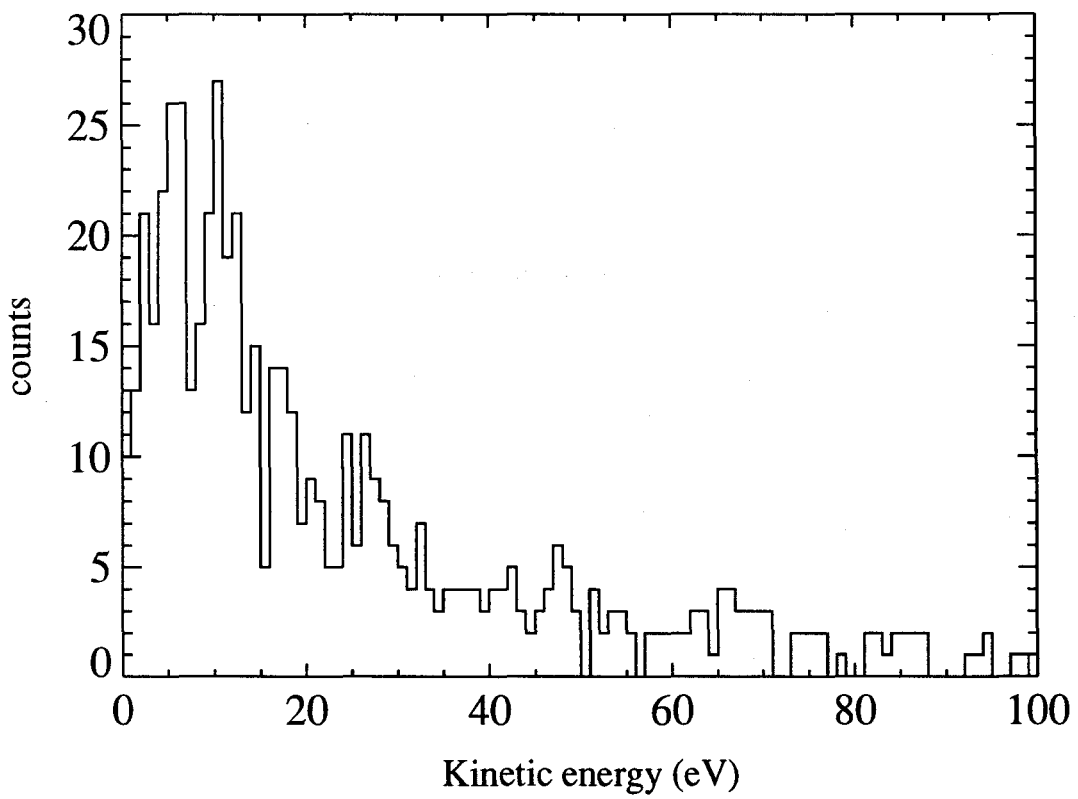

Fig. 3.2 Energy distribution of the upwards sputtered cluster atoms.

$$f(E) \approx E/(E+U_0)^3, \tag{3.2}$$

where U_0 denotes the surface escape energy barrier. For many materials this energy lies close to the sublimation enthalpy[37] (for rhodium 5.75 eV). This distribution peaks at half the escape barrier. In the calculated kinetic energy distribution the peak lies at a much higher value of about 10 eV. This shift of the peak to higher energies is probably the result of a not fully developed collision cascade.

When bombarding the surface of a close packed crystal the sputtered atoms usually originate from the surface of the sample. Exited atoms from the second layer are blocked by the surface atoms, except when moving in the direction normal to the surface. This effect is also observed in the clusters. Since all atoms are marked with a number and sorted by shell and height (as discussed in 2.4.2) we can easily keep track of where sputtered atoms originated from. In figure 3.3 the frequency at which atoms escape from the cluster is shown. The dotted vertical lines indicate the separations between the successive shells. As is clearly visible, the sputtered atoms mainly escape from the outermost shell of the cluster. Within a shell the highest atoms tend to escape upwards (detectable in SIMS). The lower atoms are preferentially sputtered downwards, where they may influence the subsequent measurements. The lowest ten atoms of the cluster (numbers 138 through 147) are bound by both the cluster and the support, they have a low sputter probability.

In SIMS the angular distribution of the sputtered atoms can be measured. For atoms sputtered from a bulk sample this distribution is well known[11]. Figure 3.4(a) shows the

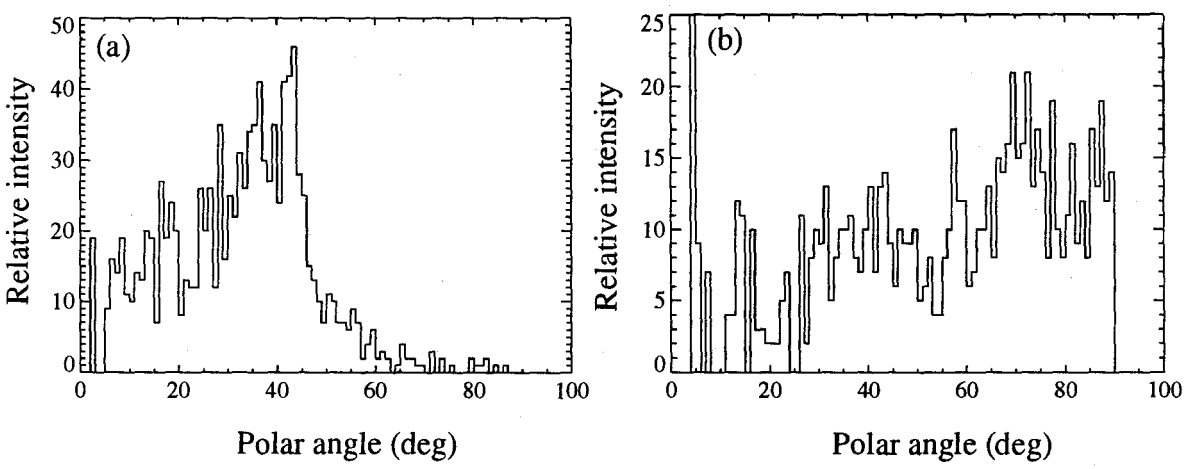

Fig. 3.4 Polar angle distributions of a) sputtered support atoms and b) sputtered cluster atoms. Atoms at angle higher than 90° are excluded. The intensities are normalized.

polar angle (angle with respect to the normal) distribution of the upwards sputtered support atoms. This profile resembles those calculated and measured for rhodium (111)[10], with a maximum at 40° and a minimum at 20°. In the support escaping atoms are forced to the normal by their neighbours, since atoms escaping at grazing angles are scattered. For the higher angles there is additional blocking by the cluster, but this effect is small. The distri-

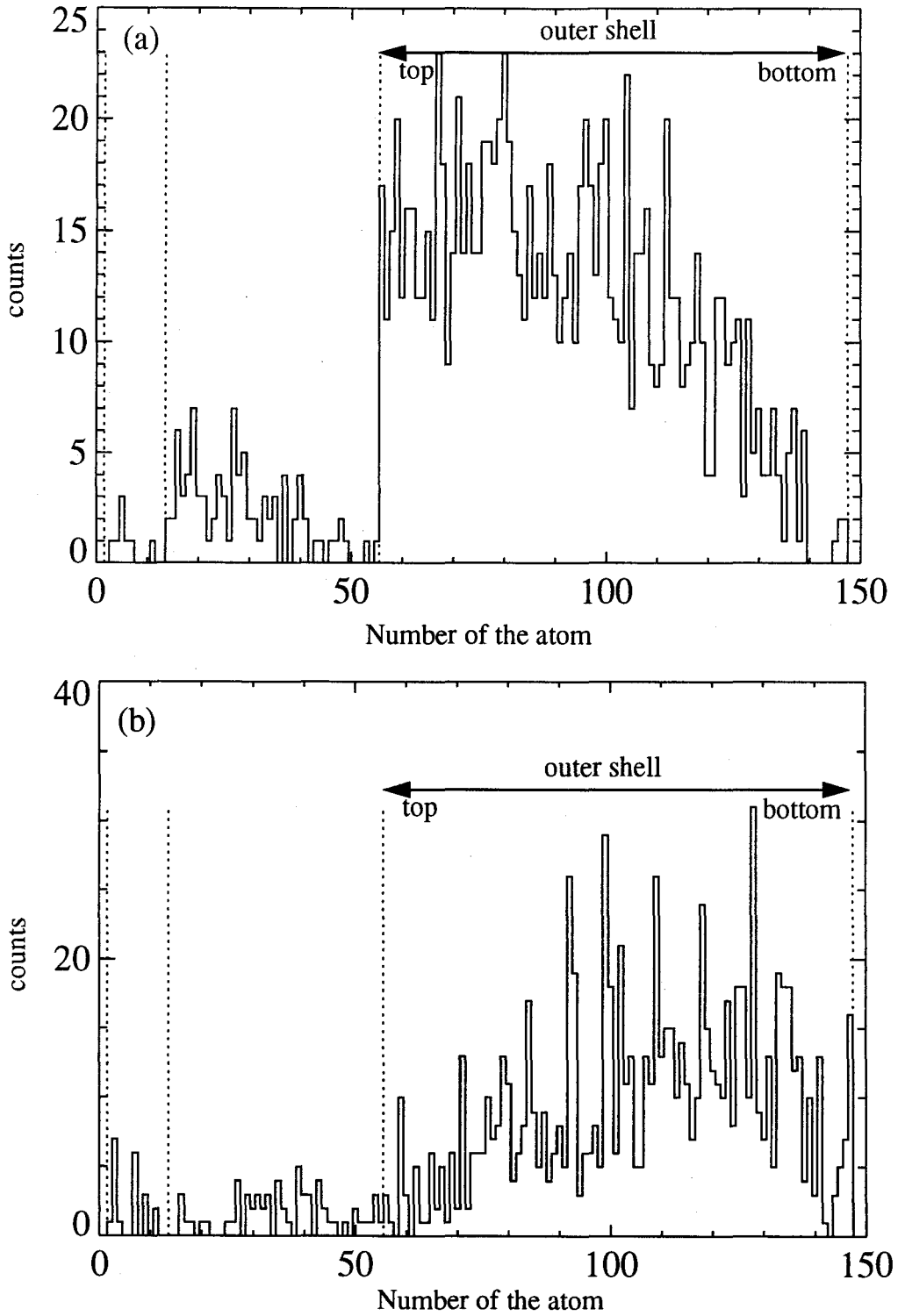

Fig. 3.3 Frequency distribution of the sputtered cluster atoms, a) upwards and b) downwards. The dotted lines mark the transitions between shells.

bution for the upwards sputtered cluster atoms is quite different, as can be seen in figure 3.4(b). The low angle part has the same shape, but at higher angles the intensity does not abruptly drop to zero. This is the result of the tilted surfaces and of the lower coordination number of most of the atoms in these surfaces.

The atoms sputtered from a crystal surface show an azimuth angle distribution[11], and so do the scattered ions[38]. This too, is explained by the structure of the surface. In certain directions the neighbour atoms are more distant, so atoms in the surface moving in that direction have a lower chance of being deflected, see figure 2.4. This preference for ejection along the open channels of the crystal is indeed observed for atoms sputtered from the support, with the peaks in intensity 60° apart, see figure 3.5(a). The blocking by the cluster

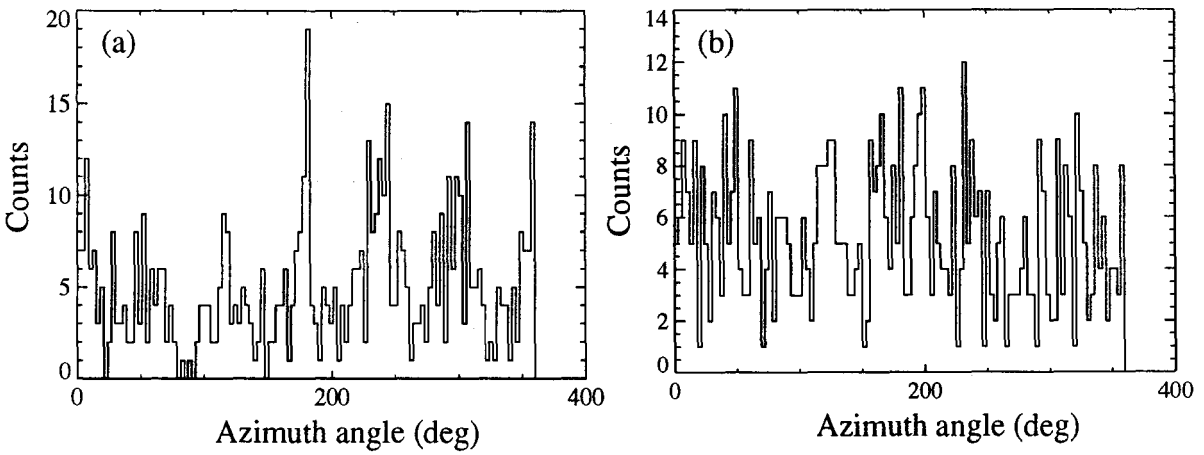

Fig. 3.5 Azimuth angle distribution of atoms sputtered from a) the support and b) the cluster. The cluster blocks the support atoms sputtered at 90°.

around 90° is clearly visible. For atoms sputtered from the cluster the pattern is less clear, as can be seen in figure 3.5(b). This can be explained by the low coordination number of the atoms in the surfaces, so they are only weakly focused in certain directions, and by the multiple surfaces of the cluster, allowing atoms to escape in all directions.

4 Conclusions

4.1 General

Rhodium clusters on a rhodium support are quite stable under low energy ion bombardment. When hit by an ion they lose a couple of atoms, but the idea of an exploding cluster turns out to be false: the cluster hardly ever loses more than a dozen atoms. Only when hit at special points the sputter yields are higher.

The number of atoms sputtered from the thin support and their distributions are in reasonable agreement with the experimental data. For the cluster the number of upwards sputtered atoms is significantly higher. Their kinetic energy distribution peaks at a twice the normal value, which is the result of a not fully developed collision cascade. Other discrepancies were found in the angular distributions. These differences are explained by geometrical effects.

Since the differences between sputtering from the cluster and from bulk can all be explained by the small size and the large surface of the cluster, we expect that similar results are to be found when sputtering from clusters with another shape or a different number of atoms.

4.2 Time dependence

In LEIS and SIMS the samples are often analysed for longer time periods. In these measurements the chances of hitting a cluster twice become significant. In the present simulations we only looked at the scattering on a fresh cluster. Because of the rhodium support it is not possible for a cluster to restore from the damage of an impact, so scattering of a second ion is not realistic. A time dependent signal might be obtained by extrapolation of the current results. When bombarded with 2 keV neon a cluster loses on the average 6.33 atoms per impact (ion impinging in area *i* or *ii*), neglecting the influence of ions impinging in area *iii*. With each impact the surface area of a cluster (or the number of scattering nuclei for LEIS) is reduced by about $1 - (1 - 6.33/147)^{2/3} \approx 2.9\%$. At the same time, on the average there appear 2.95 extra scattering nuclei on the support surface, the downwards sputtered atoms. Of these atoms a small fraction penetrates into the support. A factor that also has to be addressed in this estimation is how long the single rhodium atoms stay on the support before they are sputtered, covered by the support or re-unite with the cluster. From these considerations it is not possible to predict the nett result.

Most of the sputtered cluster atoms originate from the surface of the cluster. This can be taken advantage of when a cluster contains a mixture of atoms, like palladium and platina as in figure 1.2. The atoms with the lowest surface free energy will cover the surface and are thus sputtered first. In following hits, the second constituent then becomes more prominent. But, when atoms are sputtered from a cluster the ion has disturbed the cluster

pretty much. Due to the excess energy in the cluster the atoms have a high mobility, so the old surface composition may be restored. This effect can neutralize the effect of preferential sputtering of atoms from the surface.

5 References

1 R. Prins, dictaat Lecture notes 'Katalyse', nr 6637, TUE.

2 L.C.A. van den Oetelaar, graduation report, Eindhoven University of Technology, 1992.

3 See for instance: A.K. Datye and N.J. Long, *Ultramicroscopy*, **25** (1988), 203-208; J. Burkhardi and L.D. Schmidt, *J. Catal.*, **116** (1989), 240-251; M.J. Jacamán, D. Romeu, S.Fuentes and J.M. Dominiguez, *J. Chimie Physique*, **78** (1981), 861-866; C.Y. Yang, M.J. Yacamán and K. Heinemann, *J. Crystal Growth*, **47** (1979), 283-290.

4 See for instance: D.N. Belton, S.J. Schmieg, *Surf. Sci.*, **202** (1988), 238-254.; S.H. Oh and C.C. Eickel, *J. Catal.*, **128** (1991), 526-536.

5 L.C. Feldman and J.W. Mayer,'Fundamentals of Surface and Thin Film Analysis', North Holland, Amsterdam, 1986.

6 P. Groenen, graduation report, Eindhoven University of Technology, 1988.

7 M. Skoglundh, L.O. LÖwendahl, P.G. Menon, B. Stenbom, J.-P. Jacobs, O. van Kessel and H.H. Brongersma, *Catal. Let.*, **13** (1992), 27-38.

8 H.H. Brongersma, R.H. Bergmans, L.G.C. Buijs, J.-P. Jacobs, A.C. Kruseman, C.A. Severijns and R.G. van Welzenis, *Nucl. Instr. and Meth. B*, **68** (1992), 207-212.

9 M.W. Thomson, *Phys. Reports*, **4** (1981), 335-371; M.W. Thompson, *Phil. Mag.*, **18** (1968), 377-414.

10 B.J. Garrison, N. Winograd, D.M. Deaven, C.T. Reimann, D.Y. Lo, T.A. Tombrello, D.E. Harrison jr. and M.H. Shapiro, *Phys. Rev. B*, **37** (1988), 7197-7204.

11 R. Maboudian, Z. Postawa, M. El-Maazawi, B.J. Garrison and N. Winograd, *Phys. Rev. B*, **42** (1990), 7311-7316.

12 G.C. van Leerdam, Ph-D thesis, Eindhoven University of Technology, 1991.

13 C.A. Severijns, Ph-D thesis, Eindhoven University of Technology, 1992.

14 M.P. Allen and D.J. Tildesley,'Computer Simulations of Liquids', Clarendon Press, Oxford,1987.

15 W. Eckstein, 'Computer Simulation of Ion-Solid Interactions', Springer-Verlag, Berlin, 1991.

16 H.Feil, J. van Zwol, S.T. de Zwart, J. Dieleman and B.J. Garrison, *Phys Rev B*, **43** (1991), 13695-13698

17 Sumio Iijima and Toshinari Ichihashi, *Phys. Rev. Lett.*, **56** (1986), 616-619.

18 Ino, *J. Phys. Soc. Jpn.*, **27** 941 (1969).

19 See for instance: W. Andreoni and P. Ballone, *Phys. Scripta*, **T19** (1987), 289-297; F. Ercolessi, W. Andreoni and E. Tosatti, *Phys. Rev. Let.*, **66** (1991), 911-914; L.D. Marks, *Phil. Mag. A*, **49** (1984) 81-93 & 95-109.

20 C.Y. Yang, *J. Crystal Growth*, **47** (1979), 274-282.

21 L. Verlet, *Phys Rev.*, **159** (1967), 98

22 D.E. Harrison jr., W.L. Gay and H.M. Efron, *J. Math. Phys.*, **10** (1969), 1179-1184.

23 R. Smith and D.E. Harrison jr., *Comp. in Phys.*, sep/oct 1989, 68-73.

24 H.J.C. Berendsen, J.P.M. Postma, W.F. van Gunsteren, A. DiNola and J.R. Haak, *J. Chem. Phys.*, **81** (1984), 3684-3690.

25 M.S. Daw and M.I. Baskes, *Phys. Rev. Lett.*, **50** (1983), 1285, *Phys. Rev. B*, **29** (1984),

6443-6453.
26 M.S. Daw, *Phys. Rev. B*, **39** (1989), 7441-7451.
27 M.I. Bakses, J.S. Nelson and A.F. Wright, *Phys. Rev. B*, **40** (1989), 6085-6100.
28 S.M. Foiles, M.I. Baskes and M.S. Daw, *Phys. Rev. B*, **33** (1986), 7983-7991.
29 E. Clementi and C. Roetti, Atomic Data and Nuclear Data Tables, Academic, New York, 1974. Vol. 14, Nos. 3 and 4, p. 231.
30 J.H. Rose, J.R. Smith, F. Guinea and J. Ferrante, *Phys. Rev. B*, **29** (1984), 2963.
31 G. Molière, *Z. Naturforsch*, **2a** (1947), 133.
32 O.B. Firsov, *Zh. Eksp. Teor. Fiz.*, **33** (157), 696.
33 P.M. Morse, *Phys. Rev.*, **34** (1929), 57.
34 J. Tersoff, *Phys. Rev. Lett.*, **56** (1986), 632.
35 N. Matsunami, Y. Yamamura, Y. Itikawa, N. Itoh, Y. Kazumata, S. Miyagawa, K. Morita, R. Shimizu and H. Tawara, *Atomic Data and Nuclear Data Tables*, **31**, 1-80 (1984).
36 R. Behrisch (ed.), Sputtering by Particle Bombardment, Vol. 1, Springer-Verlag, Berlin, 1981.
37 A.J. van Roosmalen, J.A.G. Baggerman and S.J.H. Brader, Dry Etching for VSLI, Plenum Press, New York, 1991.
38 A.C. Kruseman, graduation report, Eindhoven University of Technology, 1992.

Acknowledgements

Prof.dr. H.H. Brongersma stimulated me to investigate the dynamics of ion scattering on a supported rhodium cluster and to start a cooperation with dr. Hans Feil.

Dr. Hans Feil has given me advice and the two of us shared a room and computer. During my stay I also enjoyed the company of the other members of the group Theoretical Physics of dr. P.J. Kelly.

I would like to thank Philips Electronics N.V. in Eindhoven for giving me the opportunity to do this work at the Philips Research Laboratories. Financial support of Philips is acknowledged, as well as a generous supply of computer resources.

Appendix

Table A.1: Average sputter yields per incident ion for the cluster.

Ion, energy	Area *i*			Area *ii*			Area *iii*		
	Percentage of damaged clusters	Upwards sputtered atoms	Downwards sputtered atoms	Percentage of damaged clusters	Upwards sputtered atoms	Downwards sputtered atoms	Percentage of damaged clusters	Upwards sputtered atoms	Downwards sputtered atoms
He, 0.5 keV	24	0.12	0.24	0	0	0	1	0.01	0.01
He, 2.0 keV	29	0.18	0.34	2	0.02	0	0	0	0
He, 5.0 keV	21	0.31	0.38	0	0	0	0	0	0
Ne, 0.5 keV	81	2.4	2.3	14	0.14	0.10	14	0.25	0.13
Ne, 2.0 keV	91	4.4	3.2	13	0.17	0.05	9	0.20	0.12
Ne. 5.0 keV	91	2.8	2.5	11	0.57	0.38	3	0.04	0.03
Ar, 0.5 keV	93	3.7	3.7	11	0.00	0.11	6	0.06	0.01
Ar, 2.0 keV	100	8.1	7.3	30	0.35	0.29	16	0.29	0.10
Ar, 5.0 keV	99	7.0	5.7	19	0.40	0.21	7	0.10	0.04

Table A.2: Average sputter yields per incident ion for the support.

Ion, energy	Area *i*		Area *ii*		Area *iii*	
	Percentage of damaged supports	Upwards sputtered atoms	Percentage of damaged supports	Upwards sputtered atoms	Percentage of damaged supports	Upwards sputtered atoms
He, 0.5 keV	0	0	3	0.03	9	0.10
He, 2.0 keV	0	0	6	0.08	1	0.01
He, 5.0 keV	1	0.01	6	0.13	1	0.01
Ne, 0.5 keV	13	0.25	43	0.76	46	0.80
Ne, 2.0 keV	49	0.81	49	0.92	48	1.0
Ne. 5.0 keV	35	0.96	38	0.70	35	0.59
Ar, 0.5 keV	21	0.3	59	1.1	64	1.0
Ar, 2.0 keV	65	1.9	76	2.6	80	2.1
Ar, 5.0 keV	76	2.9	59	1.3	54	1.2